MODELING AND UNDERSTANDING OF DIRECTIONAL FRICTION ON A FULLY

LUBRICATED SURFACE WITH REGULAR ANISOTROPIC ASPERITIES

A Thesis Submitted to the College of

Graduate Studies and Research

In Partial Fulfillment of the Requirements

For the Degree of Master of Science

In the Department of Mechanical Engineering

University of Saskatchewan

Saskatoon

By

Zhiming Zhang

July 2010

ABSTRACT

Traditional tribology is based on the surface with random micro structures due to limitations of manufacturing technology. The modern manufacturing technology now promises to fabricate surfaces with regular micro structures (or asperities). The word 'asperity' refers to a single physical entity on the surface of a material, contributing to a concept called roughness in traditional tribology. Regular asperity surfaces imply that all asperities on the surface of a material have the same shape and size, and a deterministic distribution over the surface. The emergence of regular asperity surfaces will have a transformative impact to the discipline of tribology.

The overall objective of this thesis is to study how the regular asperity would affect the tribological behavior. Specifically, this thesis develops a computational model to demonstrate and characterize the effect of the surface with regular anisotropic asperities (RAA) on the directional friction behavior when the surface is in a fully lubricated state. By directional friction, it is meant that friction force changes its magnitude with the change of the relative motion direction. By anisotropic asperity, it is meant that the geometry of the asperity is not symmetrical along the motion direction.

This thesis presents a detailed development of the computational model by employing computational fluid dynamics (CFD) techniques. In particular, the model takes the Navier-Stokes (NS) equation as a governing equation and the Half-Sommerfeld Condition (HSC) to represent

fluid behavior in the cavitation region; as such the model is named NS-HSC for short. Verification of the NS-HSC model is conducted with the information available in literature. A theory is proposed to explain the relationship between directional friction behavior and specific RAA structures. The thesis concludes: (1) the NS-HSC model is more accurate than the existing model in the literature and can be used to predict directional friction behavior and to design RAA surfaces, and (2) the proposed theory is excellent consistent with the NS-HSC model and thus useful to analysis and design of RAA surfaces for directional friction.

The major contributions of this thesis are: (1) the first model in the field of tribology to predict the directional friction behavior for RAA surfaces under a fully lubricated status, (2) the first investigation, in the field of CFD, into combining the NS and HSC for modeling a laminar flow with cavitation, and (3) the first theory in the field of tribology for directional friction on fully lubricated RAA surfaces.

.

ACKNOWLEDGMENTS

DEDICATED TO MY GRANDPARENTS

TABLE OF CONTENTS

LIST OF TABLES

LIST OF FIGURES

LIST OF ABBREVIATIONS

L	Length of the external area of the fluid domain, μm
L_x	Length of the asperity, no units
L_y	Height of the asperity, no units
LIGA	German acronym for **Li**thographie, **G**alvanoformung, **A**bformung
LST	Laser Surface Texturing
$p\,(x,y,z)$	Priliminary pressure distribution within the fluid domain before HSC adjustment, Pa
$P\,(x,y,z)$	Pressure distribution within the fluid domain after HSC adjustment, Pa
PDF	Partial Differential Equation
r	Radius of the cylindrical asperity, μm
R	Radius of the cylindrical unit cell, μm
RAA	Regular Anisotropic Asperity
Re	Renolds number, no units
RIA	Regular Isotropic Asperity
U	Moving speed of the upper surface with respect to the lower surface, m/s
UDF	User Defined Function
$u\,(x,y,z)$	x-direction velocity distribution within the fluid domain, m/s
$v\,(x,y,z)$	y-direction velocity distribution within the fluid domain, m/s
$w\,(x,y,z)$	z-direction velocity distribution within the fluid domain, m/s
x	Horizontal direction
$x+,\ +x$	Positive horizontal direction
$x\text{-},\ \text{-}x$	Negative horizontal direction

y	Vertical direction
z	Width direction
α	Asperity inclination angle – left, degeree
β	Asperity inclination angle – right, degree
θ	Asperity inclination angle, degree
ρ	Density of the fluid, kg/m^3
μ	Dynamic viscosity of the fluid, Pa·s
Φ (x,z)	Geometry of the lower surface

CHAPTER 1 INTRODUCTION

1.1 Background

In this thesis, the generation of directional friction on a fully lubricated surface with regular anisotropic asperities will be studied. In this section, the fundamentals of friction and lubrication, the terms of *friction uniformity* (the general concept of *directional friction*) and *surface with regular asperities* will be introduced.

1.1.1 Fundamentals of Friction and Lubrication

Friction (or friction force) is considered as a tangential force that is applied to the surfaces of two objects, and it resists the movement or the tendency of movement of one object with respect to the other object. The movement can be in the form of rolling or sliding. Friction force can be beneficial; for example, friction-induced traction is needed for a vehicle to move on a slippery road. Friction can be undesirable; for example, dragging from the road surface on the non-driving wheels of a vehicle. When friction is undesirable, reduction of friction is a common objective. One of the ways to reduce friction is to separate two contacting objects, creating a "floating effect" using a medium (gas, liquid or solid particles). The material of such a medium is called a lubricant. Such a method to reduce friction is called lubrication in tribology.

There are different lubrication states: clear surface (with no lubrication) state, boundary lubrication state, mixing lubrication state, hydrodynamic lubrication state, elasto-hydrodynamic lubrication state and static lubrication state [Bhushan, 2002]. In this thesis, the clear surface (with no lubrication) state and the boundary lubrication state (when the lubricant is not intentionally brought in between two solid objects) are called non-lubricated states in general. The hydrodynamic and elasto-hydrodynamic lubrication state and static lubrication state are called fully-lubricated states in general. The following will introduce only the non-lubricated state and fully lubricated state, as they are the most relevant to the work presented in this thesis.

In a non-lubricated state, there are solid contacts between the surfaces of two solid objects. The normal load between these two solid surfaces is taken by these solid contacts, and the friction force comes from the interactions of these two contacting surfaces.

In a fully lubricated state, there is no solid contact between two solid objects. The surfaces of these contacting objects are completely separated by lubricants. The normal load on the solid surface is taken by the lubricant pressure. The friction force in this case comes from the tangential drag of the lubricant on the surface. The lubricant pressure has two different sources: static pressure from an external pump and hydrodynamic pressure from the motion of the surface. The lubrication method based on static pressure is named hydrostatic lubrication, and the lubrication method based on hydrodynamic pressure is named hydrodynamic lubrication. If the deformation of the solid surface due to the hydrodynamic pressure is also taken into consideration, then this type of hydrodynamic lubrication is specifically called elasto-hydrodynamic lubrication. In this thesis, hydrodynamic lubrication is considered.

Fig. 1.1 shows a basic configuration of hydrodynamic lubrication. There are two surfaces in this configuration: the lower one which is assumed to be fixed and the upper one which is traveling towards right with speed U. There are lubricants between these two surfaces, and the two surfaces form a wedged gap. The movement of the upper surface keeps dragging the fluid into the narrow end of the gap and thus creates the hydrodynamic pressure P within the lubricant. In Fig. 1.1b, a sketch of the pressure distribution on the upper surface is shown. Pressure P separates the two surfaces and generates a lifting force F_l on the upper surface and pushing force F_p on the lower surface. There is a drag on the upper surface from the fluid, which is tangential to the upper surface and is opposite to the motion direction of the upper surface. This drag is named friction force F_f, and it is a main concern of this thesis research. The magnitude of the friction force is related to the velocity distribution of the lubricant between the two surfaces.
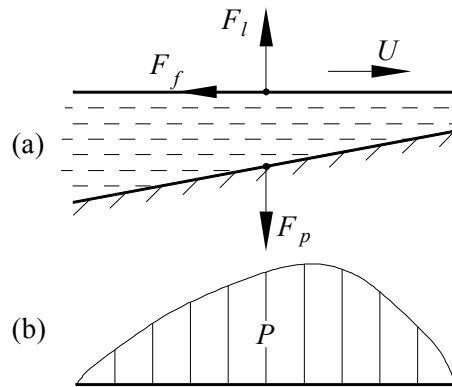
Fig. 1.1 Hydrodynamic lubrication configuration

1.1.2 Friction Uniformity

Friction forces on most contacting surfaces, whether they are in a lubricated state or not, are

3

assumed to be uniform. That is to say, the magnitude of the friction force is independent of (1) the relative motion direction; and (2) the location where the friction takes place. This assumption, though accepted in standard texts for a long time, is however not always true. There are experiments that have shown the non-uniform friction behavior (i.e., the magnitude of the friction force depends on the relative motion direction and/or the location) on natural material surfaces like wood [Ohtani et al., 2003], snake skin [Hazel et al., 1999], on a surface with irregular anisotropic asperities [Rhaiem et al., 2004; Chvedov et al., 2003], on the surfaces of single crystal materials, ceramic materials, and composite materials [Gatzen and Beck, 2003; Mancinelli and Gellman, 2004; Yamamoto and Hashimoto, 2004], and on the surfaces with a much smaller size range of asperities (e.g., on a single carbon nanotube surface [Lucas et al., 2009]). These observations can lead to the notion of *non-uniform* friction. The term *Friction Uniformity* is used to describe the property of the friction force, in particular whether the friction force is uniform or not.

Among all non-uniform friction phenomena, those dependent only on the sliding direction are further called *directional friction* or anisotropic friction [Zmitrowicz, 2006] and those dependent on the friction location are called *heterogeneous friction* [Zmitrowicz, 2006].

Fig. 1.2 summarizes the classification of friction as discussed so far. The property adopted to distinguish different classes of friction here is termed *friction uniformity*. This thesis will focus on the directional friction in particular.

```
                        ┌──────────┐
                        │ Friction │
                        └──────────┘
              ┌──────────────────┐   ┌────────────────────┐
              │ Uniform Friction │   │ Non-uniform Friction│
              └──────────────────┘   └────────────────────┘
        ┌─────────────────────────┐   ┌───────────────────────────────────────┐
        │ Heterogeneous Friction* │   │ Directional Friction/Anisotropic friction* │
        └─────────────────────────┘   └───────────────────────────────────────┘
```
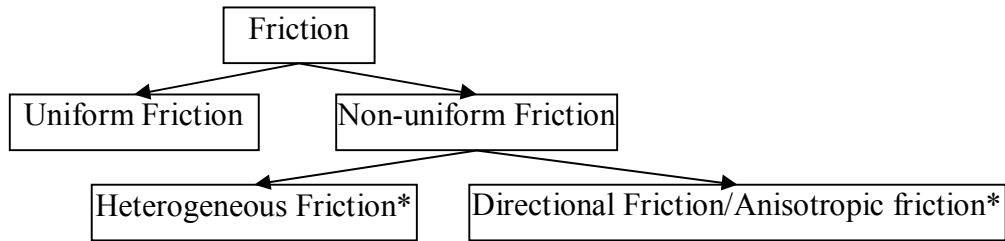
Fig. 1.2 Classification of friction
The terms with * was proposed by [Zmitrowicz, 2006]

1.1.3 Surfaces with Regular Asperities

When viewed at different scales (macro, micro or nano), different geometries on the same surface can be observed. For example, an engineered surface may look shiningly flat at the macro scale with naked eye; while it may show "hill and valley" like structures at the micro scale under the microscopy with a micron level resolution. Similarly, the seemingly flat surface viewed at the micro level may show "hill and valley" like structures when viewed under microscopy with a nano level resolution. These "hill and valley" like micro/nano structures are named *asperities* in this thesis, and this thesis only concerns the micro asperities.

Asperities on engineered surfaces fabricated with conventional methods such as turning, milling, and so on are irregular, which means that these asperities have non-determined shapes and sizes, and their distribution on the surface has a random fashion. In recent years, newly developed techniques are able to fabricate a surface with *regular asperities* that have determined shape, size and distribution pattern. For examples, Stephens et al., [2004] fabricated a surface with LIGA (German acronym for **Li**thographie, **G**alvanoformung, **A**bformung) process (Fig. 1.3a). It has a series of asperities that have the same shape (hexagonal prism), same size (7

5

micros in height, 550 microns in diameter) and determined distribution pattern (hexagonal as well). Wang et al. [2001] fabricated a ceramic surface with the LST (Laser Surface Texturing) process (Fig. 1.3b). It has a series of dimples that have the same cylindrical shape, size (200 microns in diameter and 10 microns in depth) and determined distribution pattern (linearly distributed). Petterson and Jacobson [2006] fabricated a surface with lithography, molding and CVD (chemical vapor deposition) processes (Fig. 1.3c). It has a series of diamond asperities that have the same shape (pyramid), size (100 microns in width and about 50 microns in height) and determined distribution pattern (linear). Beside these examples, there are many other sample surfaces that have regular asperities, and they will not be listed one by one here for the sake of brevity.
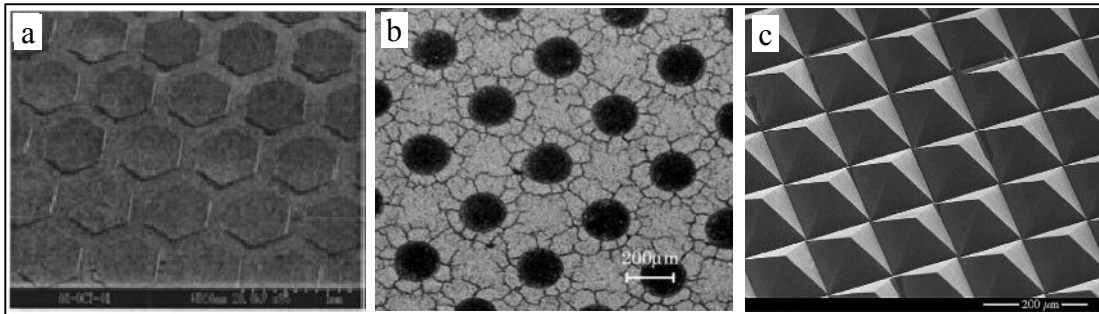
Fig. 1.3 Surfaces with regular asperities
[a. Stephens et al. 2004; b. Wang et al., 2001; c. Petterson and Jacobson, 2006]

As well, the above samples show: the shape of the asperities can be cylindrical or pyramid structures and further, the shape can be either concave (Fig. 1.3b) or convex (Fig. 1.3a and c). The concave micro structure is also accepted as a kind of asperity in this thesis. The particular size (height/depth) of the asperities in these examples ranges from 7 to 50 microns.

In this thesis, only when the size (height/depth) is within the range from 1 micron to 50 microns, will the asperities be considered as the micro regular asperity. This is because the micro structure loses the sense of asperity when its size is larger than 50 microns, and it can no longer be considered as a micro asperity but can only be considered as a feature or geometrical structure in a more general level. When the size of asperities is smaller than 1 micron, they are not considered as micro asperity either, as their friction behavior follows a completely different law other than that for the asperity at the micron level. This consideration is consistent with the concept of roughness in the contemporary manufacturing technology.

Further, it can be found that all the asperities shown in Fig. 1.3 are axially symmetric, and they are called in this thesis *regular isotropic asperity* (RIA). If the asperities are not axially symmetric, they are called *regular anisotropic asperity* (RAA) surface. Fig. 1.4 shows an example of the surface with RAAs [Tang et al., 2010]. The surface is fabricated with a combined HF-CVD and IBE (ion beam etching) method.
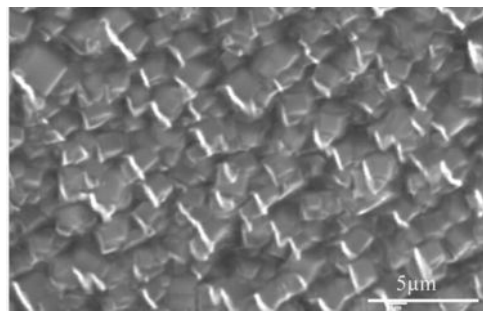
Fig. 1.4 Surface with regular anisotropic asperities [Tang et al., 2010]

1.2 Motivation

As mentioned in section 1.1.1, there are contacts between two solid surfaces in the non-lubricated condition, and the friction force comes from interactions between the two surfaces in contact. Specifically, these interactions come from adhesion and blockage of the asperities on the surfaces in contact. The concepts of asperities are described in section 1.1.3. The interactions of these asperities are the key factors that produce the friction phenomenon in the non-lubricated condition. In fact, the same asperities will also change the tribological behavior on the surface in a fully lubricated state. The changed tribological behavior includes friction force and load capacity on the surface. This is because the presence of the asperities may change the flow properties (velocity, direction, etc.) between the two surfaces and may form wedged gaps between the two surfaces, which will further lead to the hydrodynamic effect.

Conventional tribology only considered two fundamental properties of friction force, namely, magnitude and direction. In section 1.1.2, a new concept Friction Uniformity was introduced, and it is considered as a new property of friction force. In particular, friction uniformity, though based on the two fundamental properties of friction force, describes the way of changing the magnitude of friction force with respect to the location and/or the direction of the surface motion (see section 1.1.2). The study of friction uniformity will provide a more fundamental understanding of the friction behavior. It is believed that asperities on the surface (lubricated or not) will change the magnitude and direction of friction force and further change the uniformity of friction force.

Traditional tribology is based on the surface with irregular asperities. By its very nature, the distribution, size and shape of asperities are random. In order to describe the 2D or 3D micro-geometry of these surfaces, statistical-based models such as those mentioned in [Longuet Higgins, 1957; Greenwood and Williamson, 1966; Greenwood 1984] are used. Or more simply, the engineering concept called "roughness" is used in industrial applications to a very large extent, which measures the average height of asperities or the average "altitudes" of asperities at different locations on the surface. The tribological properties that occur on the surfaces are controlled approximately by controlling the roughness of these surfaces. Therefore, irregular asperities are not individually considered, but a group of asperities will make sense. In contrast, the micro-geometry of a surface with regular asperities (as introduced in section 1.1.3) can be described in a determined fashion, as the size, shape and distribution of asperities are regular. Therefore, regular asperities can be individually considered, and the tribological behavior on the regular surfaces can be controlled by controlling the size, shape and the distribution of the asperities on the surfaces, whether it is in a fully lubricated state or non-lubricated state.

It is very important and interesting to understand how regular asperities (in terms of shape, size and distribution) would affect the tribological behavior on surfaces in different lubrication states. This is the fundamental question that motivates the research of this thesis. However, knowledge to potentially generate answers to this question involves many aspects of tribology. This is because each term (regular asperity, tribological behavior and lubrication state) used in relation to this question includes different aspects or classifications. Fig. 1.5 attempts to show all aspects that surround this question. In the thesis, however, only a part of the aspects will be considered (those in dashed red lines shown in Fig. 1.5, and they will be explained later).
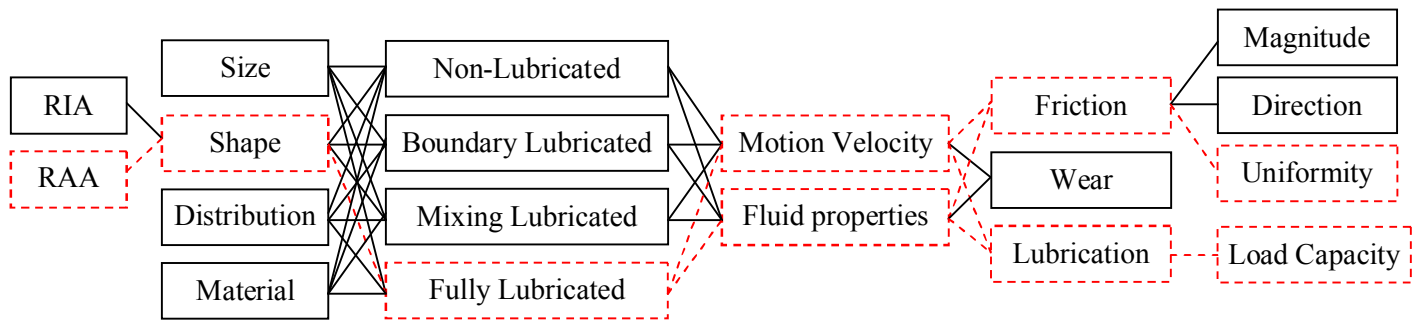
Fig. 1.5 Aspects of knowledge related to regular asperity surface
(Colored in e-version)

In the proposal for a NSERC (**N**ature **S**cience and **E**ngineering **R**esearch **C**ouncil of Canada) grant submitted by Zhang et al. [2004], it was hypothesized that friction force will exhibit directional behavior on the surface with regular anisotropic asperities (see Fig. 1.6, when $\alpha \neq \beta$). That is to say, the anisotropy of the regular asperity will change the friction uniformity. The hypothesis has been proven by experiment in [Zhang, 2008], which shows that friction force is directional on the surface with RAAs in a non-lubricated state. This thesis answers the question**: will this hypothesis be valid on a surface with RAAs in a fully lubricated state?**
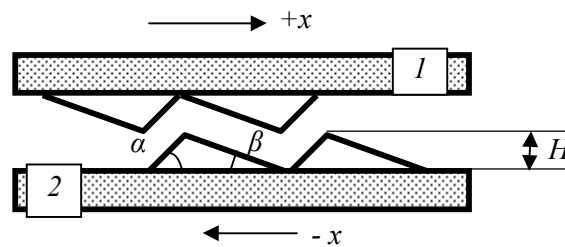
Fig. 1.6 Surface with regular anisotropic asperities

There are two methods with which to generate an answer to the above question: by model or by experiment. If the question is going to be answered by a model, a further question is: **how to**

model friction force on the surface with regular anisotropic asperities in a fully lubrication state? Furthermore, this thesis also aims to understand **would the shape of the RAAs affect the friction uniformity, directional friction in particular**. The study in this thesis was motivated to answer these questions. The boxes and the dashed lines coloured in red shown in Fig. 1.5 give a scope of the study described in this thesis.

1.3 Objectives

To answer the three questions described in section 1.2 above, this study was designed to have the following objectives:

Objective (i): *Establish a model which can compute the friction force and lifting force on a fully lubricated RAA surface.* The model will be based on the structure of two contacting surfaces. One of the surfaces is flat, and the other has RAAs on it. The distance between these two surfaces and the height of the asperity are of the same order. The model will be able to compute the friction force and the lifting force on the surface which is flat when it is traveling in two opposite directions with respect to the other one; see Fig. 1.7 for a visual impression.
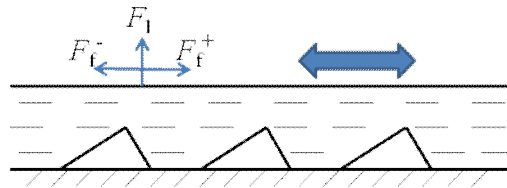
Fig. 1.7 Configuration of the flow domain concerned in the proposed objective

Objective (ii)*: apply the model to be developed in objective (i) to a fully lubricated surface with RAAs and compute the friction force*. If the friction force along one direction is different from its opposite direction, the hypothesis discussed in section 1.2 becomes true on a fully lubricated RAA surface.

Objective (iii)*: study the effect of the shape of the RAA on the friction uniformity based on the model to be developed in objective (i)*. There are two purposes with this objective: a) to better understand the effect of the RAA on friction force (particularly friction uniformity); b) to further verify the developed model. This objective will be studied by applying the model on surfaces with RAAs in different shapes and compute the friction force on them.

Objective (iv): *study the mechanism to account for why and how the surface with RAAs is able to cause the directional friction in a fully lubricated state.* If directional friction is proven to be feasible in objective (ii), the current objective is to give a discussion which may explain why it is feasible. This is useful to guiding the design of the asperities to achieve the optimal directional friction behavior.

1.4 Organization of the Thesis

This thesis consists of 6 chapters. The subsequent chapters are organized as follows:

Chapter 2: Review of related works

The general purpose of this chapter is to further justify that the research objectives proposed in

chapter 1.3 is new. In order to realize this purpose, the studies in the current literature related to friction uniformity, regular asperity surface and its effect on tribological behavior, and modeling of inter-asperity flow will be reviewed in this chapter.

Chapter 3: Model development

The general purpose of this chapter is to establish a model that can compute friction force and lifting force applied to the upper surface due to motion and to presence of the lubricant. This purpose is realized by introducing the assumptions of the described problem, determining the governing equation, setting up the boundary conditions and giving the mathematical expression.

Chapter 4: Model verification

In this chapter, the model will be verified before it will be used for the directional friction study. The verification is done by comparing the model predicted result with the experimental result from the literature. Interesting results will be discussed.

Chapter 5: Directional friction

In this chapter, the model developed and verified will be applied on the surface with RAAs which have different shapes: square cross-section and triangular cross-section. The result will be used to demonstrate the feasibility of directional friction on a fully lubricated surface with RAAs. Two theories will be proposed in the discussion of the mechanisms for directional friction for

RAA surfaces in a fully lubricated state.

Chapter 6: Conclusion and future work

In this chapter, an overview of the thesis will be presented, the conclusion and the contribution of this thesis will be given, and the future work following this thesis will be discussed as well.

Overall, chapter 3 and 4 describe the work relevant to objective (i), (ii), and (iii). Chapter 5 describes the work relevant to objective (iv).

CHAPTER 2 RELATED WORK

2.1 Introduction

The study of this thesis was focused on modeling of directional friction on a fully lubricated surface with RAAs and the effect of RAAs on directional friction. In the current literature, the work related to this focus includes those on friction uniformity (particularly the directional friction), the tribological properties of the regular asperity, and the modeling of inter-asperity flow with consideration of film rupture (or cavitation phenomenon). In this section, the related work will be reviewed and commented on.

2.2 Friction Uniformity

The current research on friction uniformity has undergone four stages of development. In the first stage, research focuses on observation of the non-uniform friction phenomenon. In the second stage, research focuses on modeling of friction uniformity. In the third stage, research focuses on realization of the non-uniform friction by fabricating the surface under human control. In the fourth stage, researches focus on application of the non-uniform friction.

In the first stage, many non-uniform friction phenomena have been observed on the surfaces of different materials. For example, Ohtani et al. [2003] observed directional (anisotropic)

friction on the wood; Hazel et al. [1999] observed directional friction on the snake skin surface; Gellman and Ko [2001] observed anisotropic friction on a pair of Ni (100) surface; Mancinelli and Gellman [2004] observed anisotropic friction between two Pd(100) crystal surfaces; Yamamoto and Hashimoto [2004] observed friction directionality on the polymeric matrix composite material and Hutton et al. [2001] observed directional friction on the ceramic- and carbon- matrix composite material; in the micro/nano- level, Hisada and Knobler. [2002] observed friction anisotropy in glycerol ester mono-layers; Dickrell et al. [2005] observed that the directional friction will be presented on the film which is formed by layers of carbon nanotube due to the nano-tube orientation and Lucas et al. [2009] observed that the AFM detected friction force is two times larger when the tip of a Atomic Force Microscopy (AFM) tip is sliding along the transverse direction on the carbon nano-tube surface than the longitudinal direction.

In the second stage, a few studies in the literature considers the modeling of directional friction. Among these few studies, Zmitrowicz as a pioneer has conducted a series of modeling studies directional friction. In [Zmitrowicz, 1981], the author formulated a model to calculate friction force on the contacting surface with isotropic and anisotropic random roughness. In the model, friction force – which is anisotropic – is calculated by multiplying a tensor called friction tensor with a velocity vector. The friction tensor is developed based on the Coulomb friction model and a rule for the generation of the friction tensors with respect to different anisotropic asperity structures. In [Zmitrowicz, 1992], the author further formulated a constitutive equation for anisotropic dry friction with tensors which depend on the sliding directions. This constitutive equation describes the so-called centrosymmetric and non-centrosymmetric anisotropic friction.

In [Zmitrowicz, 1999], the author further presented a non-homogeneous anisotropic friction constitutive equation with consideration of sliding path curvature effects. Further in [Zmitrowicz, 2006], advanced constitutive models, which describe evolutions of frictional anisotropy and heterogeneity induced by sliding kinematics was presented. First-, second- and higher-order constitutive equations of friction were developed with respect to powers of a sliding path curvature. He and Curnier [1993] formulated a model of anisotropic dry friction between two orthotropic surfaces undergoing large displacements and small strains. Morz and Stupkiewicz [1994] developed an anisotropic friction model based on Coulomb friction and the surfaces with anisotropic layout of asperities under elastic interactions. Additional to the directional friction models based on the surface with micro-level asperities, there are also few models that can simulate the atomic level anisotropic friction. In [Ohzono and Fujihira, 2000], the authors simulated a rigid gold slider with a single atomic protuberance sliding over a hexagonally packed organic monolayer of straight-chain molecules with the method of molecular dynamics, and friction anisotropy is observed at the temperature of 50K . Qi et al. [2002] conducted a series of molecular dynamic simulations at the temperature of 300K for sliding of a Ni (001)/Ni (001) interface under constant shear force; different friction coefficients are observed along different sliding orientations.

In the third stage, there have been only a few studies. Moronuki et al. [2001] fabricated a surface on silicon substrate by wet etching. During the etching process, due to the anisotropic property of the crystal silicon, the surface after wet etching has an anisotropic structure. The directional friction can be observed on this surface. Rhaiem et al. [2004] fabricated a surface on small blocks of Polyamide PA66 by milling with different surface roughness along two

orthogonal directions. The experiment and finite element simulation demonstrated the directional friction behavior on this surface. Tang et al. [2010] fabricated a surface on a silicon substrate by HF (Hot Filament) CVD and ion beam etching (IBE) techniques (see Fig. 1.4). By HF-CVD, the silicon substrate grows out a series of diamond grains. By IBE, the diamond grain was etched into the anisotropic shape. The experiment shows the directional friction behavior on the surface. By careful manipulation, the degree of anisotropy of the surface can be controlled. Furthermore, the surface discussed in [Murphy et al., 2007] also shows directional friction in the experiment. At the nano scale, Zhang and Kyriakos [2009] treated the silicon surface with oblique Ar+ ion beam irradiation, and the surface exhibits directional friction under the measurement of surface force microscopy (SFM), and difference of the friction force is load dependent.

For the fourth stage, the application of friction uniformity (particularly directional friction) concept can be found in the vibratory feed mechanism [Okabe et al., 1988], capsule robot [Yim and Jeona, 2009] and Piezoelectric Stick Slip Actuator [Zhang, 2008]. It is also expected to be applied in Carbon Nano Tube (CNT) manipulation [Lucas et al., 2009].

In conclusion, (1) friction uniformity and its modeling are not explicitly discussed in the literature; (2) many studies concern regular isotropic asperities and their affect on tribology, but there are only a few studies concerning regular anisotropic asperities. Perhaps, Zhang [2008] and Aksak et al. [2009] are the only two studies which consider regular anisotropic asperity surfaces; (3) among the studies in the literature related to friction uniformity, they all concern non-lubricated friction and/or on the surface with irregular asperities. The study concerning the regular asperity in a fully lubricated state has not been found in the literature.

2.3 Regular Asperity and Its Effect on Tribology

In this section, research about a surface with regular asperities and its tribological effect will be reviewed. The research will be divided into two categories: those concern the surface with concave asperities (see Fig. 1.3a and 1.3c) and those concern the surface with convex asperities (see Fig. 1.3b). The surface with concave asperities has less low "altitude" areas and it is fabricated with material removal methods such as LST. The surface with convex asperities has less high "altitude" areas and is fabricated with material deposit methods or mixed methods (deposit and removal) such as LIGA process, UV lithography based process, and combined CVD and IBE processes.

For the surface with concave regular asperities, LST is the most popular method. Many studies reported this method including [Wang et al., 2001; RYK et al., 2002; Kovalchenko et al., 2005; Feldman et al., 2006; Sakata et al., 2009]. In these methods, the theoretical and/or experimental results show that the LST surface will improve the tribological behavior of the surface in terms of friction reduction (due to the hydrodynamic effect), wear reduction (the micro dimples can store lubricant and provide lubricant when the surface is oil starved) and reduce the leakage of a seal. Beside LST, there are also other methods to fabricate a surface with concave asperities. For example, Ike [1996] fabricated a surface with concave regular asperities on a mental sheet using the coin approach. The mold for the coin was fabricated with ion beam etching, Wang and Kato [2003] fabricated a surface with concave regular asperities on the SiC substrate based on the reactive ion etching technique. The experiment on this surface has shown that the textured surface has a great reduction of friction force under the lubrication of water. A

more detailed review of such surfaces can be found in [Etsion and Halperin, 2005]. However, it is worthwhile to be note that all of these concave asperities in the above researches are isotropic.

For a surface with convex regular asperities, there have been only a few studies. This is perhaps because of the difficulties of fabricating convex regular asperities on a surface. Among them: Ando and Ino [1998] fabricated a surface with sinusoidal shaped regular isotropic asperities on a silicon substrate with focused ion beam milling. The height of the asperity was 49.2 nm maximum. The tribological properties such as pulling force and friction force were studied with an AFM, which has a single tip sliding on the surface. The result shows anisotropic friction on this surface. One author later [Ando, 2000] fabricated a surface with gold pyramid shaped regular isotropic asperities, and the asperity had a height of 25 microns and a width of 50 microns. Stephens et al. [2004] fabricated a surface with an array of regular hexagonal-prism-shaped asperities (average diameter: 550μm, height: 10μm, Fig. 1.2a). The experiment showed that the full-film lubrication can be realized in the thrust bearing with this surface and the friction coefficient can be reduced by 14-22%. Petterson and Jacobson [2006] fabricated a surface with regular isotropic asperities based on the UV lithography approach. The fabricated surface had arrays of pyramid shaped diamond asperities with a height of 60 microns and width of 100 microns. The fabricated surface was used to emboss flat surfaces to form concave asperities on the new surfaces where the tribology properties are improved. Shastry et al. [2006] fabricated a surface with square shaped isotropic asperities based on the UV lithography approach, and each asperity has a 50×50 microns cross-section and is about 60 microns tall. The experiment showed that this kind of surface has a strong hydrophobic property, and with careful design it can be used to guide the motion of a water droplet. As previously mentioned, Tang et al. [2010] fabricated a

surface with regular anisotropic asperities using the combined CVD and IBE techniques. A ball-on-disk dry friction test on the surface showed that friction force is obviously different when the ball slides along two opposite directions on the disk. Shi et al. [2008] proposed a non-melting laser texturing method, and this method is expected to form regular isotropic asperities by heating up particular spots of the surface with a laser. Due to the free expansion of heated areas being restricted by the surrounding cool material, the heated areas bumped up to form the convex regular isotropic asperities. A simulation based on finite element method has proved the feasibility of this method.

In conclusion: (1) Most tribology studies are based on an irregular surface with random roughness (irregular asperity) except for Tang et al. [2010] and Stephens et al. [2004], and the study of Stephens et al. [2004] is based on the RIA surface and is not related to friction uniformity; (2) Almost all the regular-asperity-related studies concerning friction uniformity are based on dry friction. The wet friction has been studied on the concave asperity surface and convex asperity surface in Stephens et al. [2004] and Shastry et al. [2006], respectively, but they are not related to friction uniformity.

2.4 Modeling of Inter-Asperity Flow and Film Rupture

The problem discussed in objective (i) in section 1.3 can be interpreted as how the surface micro geometry will affect the friction drag in a micro-fluidic device. This research involves the inter-asperity flow, as the distance between two surfaces and the height of the asperities are of the same order and the lubricant fluid is forced to flow through and over the asperities. If the fluid is viscous, when it flows from a convergent gap into a divergent gap, there will be

cavitation (bubbles) within the area at the beginning section of the divergent gap or even at the remaining section of the divergent gap if the Reynolds number is high enough. This phenomenon has been observed by experiments for some micro structures. In [Mishra and Peles, 2006], the cavitation bubbles can be observed in a micro-Venturi at the divergent end with a Reynolds number no larger than 750. In [Mishra and Peles, 2005], the cavitation was also observed after the flow passes through the micro orifice. In the research discussed in objective (i), the upper surface and the surfaces of the asperities form a series of connected convergent gaps and divergent gaps. When the fluid is dragged by the upper surface and flows from the convergent gap into the divergent one, it is believed that there could be some cavitation. This hypothesis is further supported by the experiment of [Qiu and Khonsari, 2009], where the cavitation bubbles were found on a fully lubricated surface with laser surface textured pockets. Further to their work, the Reynolds number was less than 10 and the surface speed was less than 0.8 m/s.

Therefore, in order to establish the model specified in objective (i), not only selection of the governing equation but also the cavitation problem should be considered. In the current literature related to inter-asperity flow, Matteescu et al. [1999] studied the hydrodynamic effect on fully lubricated surfaces with regular concave asperities (i.e., pockets). The 2-D Navier-Stokes (NS) equation was used as the governing equation and cavitation was not considered in their research. Harp and Salant [2001] proposed a universal average Reynolds equation capable of predicting the combined effects of inter-asperity cavitation and macroscopic cavitation. The model is based on the average Reynolds equation formulated using Patir and Cheng's methods and JFO (Jakobsson-Floberg-Olsson [Jakobsson and Floberg, 1957; Olsson, 1965]) boundary condition. In [Stephens et al., 2004], a theoretical model was developed for the RIA surface. The model is

based on the Reynolds equation with the cavitation area modeled by the half-Sommerfeld condition and the result predicted by the model has a maximum 38.2% difference with the experimental result. In [Siripuram et al., 2004] the same model used in [Stephens et al., 2004] was adopted. Based on this model, surfaces with different regular asperity shapes, asperity area ratios, load capabilities, friction coefficients and other friction properties have been tested. Brajdic-Mitidieri et al. [2005] developed a CFD (Computational Fluid Dynamics) model for simulation of the effect of the concave asperities on the pad bearing performance. In this model, the NS equation was used as a governing equation. The cavitation was considered in this model by a density based cavitation model. Sahlin et al. [2005] and Sahlin [2005] studied the influence of micro-patterned surfaces on hydrodynamic lubrication of two parallel walls. In their study, a concave regular asperity both in the isotropic condition and anisotropic condition was used. The NS equation was used as the governing equation and the cavitation problem was not considered in their study. Schweizer [2009] proposed a model based on the Reynolds equation and JFO boundary condition; the formulations of the governing equation as well as the JFO boundary condition were developed. Qiu et al. [2009] developed a model to predict the cavitation of flow on a surface with regular concave asperities. The cavitation and fluid flow are modeled by the JFO model and Reynolds equation, respectively.

From the above discussion, it can be seen that the Reynolds equation and NS equation are frequently used to govern the fluid flow. Among them, the NS equation is more general and can be used in flow with different Reynolds numbers. The half-Sommerfeld condition, Reynolds condition and JFO condition are used as boundary conditions for the cavitation area. The three approaches to model cavitations are usually used along with the Reynolds equation. For the NS

equation, there are two solutions, one is based on multi-phase flow model and the other is based on the density based cavitation model introduced in [Brajdic-Mitidieri et al., 2005]. From the literature review, there has yet to be a study for a fully lubricated surface with RAAs.

2.5 Summary

In this chapter, works related to friction uniformity, regular asperity surface and its effect on tribology, and modeling of inter-asperity flow and cavitation were reviewed. It is found that:

(1) There are many works related to friction uniformity, but they mostly concern the friction uniformity observation, and there are few works that are related to modeling and they are for the irregular asperity surface in a non-lubricated condition.

(2) There are many works related to regular asperity surfaces, but almost all the works are based on the regular isotropic asperities. Only two studies were found related to the surface with regular anisotropic asperities, but they are studied for a non-lubricated condition;

(3) In modeling of inter-asperity flow, the NS equation and the Reynolds equation are two frequently used governing equations in the current literature. If the Reynolds equation is used, the half-Sommerfeld condition, Reynolds condition and JFO condition are used to deal with the film rupture; however if the NS equation is selected, the density based model and the multiphase flow simulation are used.

Overall, the research questions and objectives, as proposed in Chapter 1, have yet to be tackled

in the current literature, especially for a fully lubricated RAA surface.

CHAPTER 3 MODEL DEVELOPMENT

3.1 Introduction

In this chapter, a mathematical model will be established to compute friction force and lifting force on a "flat" surface that moves relative to another surface with RAAs in a fully lubricated condition. First, the problem of developing this model is further clarified and set up (in Section 3.2). Second, the assumption for the model formulation is discussed (in Section 3.3). After these two steps, the governing equation and boundary condition are discussed in Section 3.4 and Section 3.5, respectively. Section 3.6 gives a full list of the mathematical expressions of the model. There is a summary in Section 3.7.

3.2 Problem Description

As described in Chapter 1 regarding objective (i), the model will be established based on a fully lubricated surface with RAAs. Fig. 3.1 shows a physical set-up of the modeling problem to be tackled, where there are two surfaces (lower one and upper one) facing each other and fully separated by a layer of lubricant film. There are regular anisotropic asperities on the lower surface (see Fig. 3.1, especially the schematic of the RAAs on the surface), while there is no asperity on the upper surface, which is hereafter called the "flat" surface. The word "flat" should be interpreted as the situation where the size of asperities is at the nano scale according to the

previous discussion in Chapter 1. By selecting these two surfaces (one flat, one with RAAs), it is enough to examine whether the directional friction can be realized or not on the fully lubricated RAA surface, and it will facilitate the analysis in later sections, which serves to find out the mechanism why directional friction is realizable or not. The result from these two surfaces will be able to give clues to a similar question where both of these two surfaces have RAAs (this point will be discussed later in Chapter 5). The lubricant region or domain between the two surfaces has four openings around the edges of the surface. The lubricant can flow in and flow out through the openings without any constraint from the external environment. The lower surface is considered to be stationary and the upper surface can travel on the top of the lower surface on two opposite directions, namely the +x and the –x direction (Fig. 3.1b).
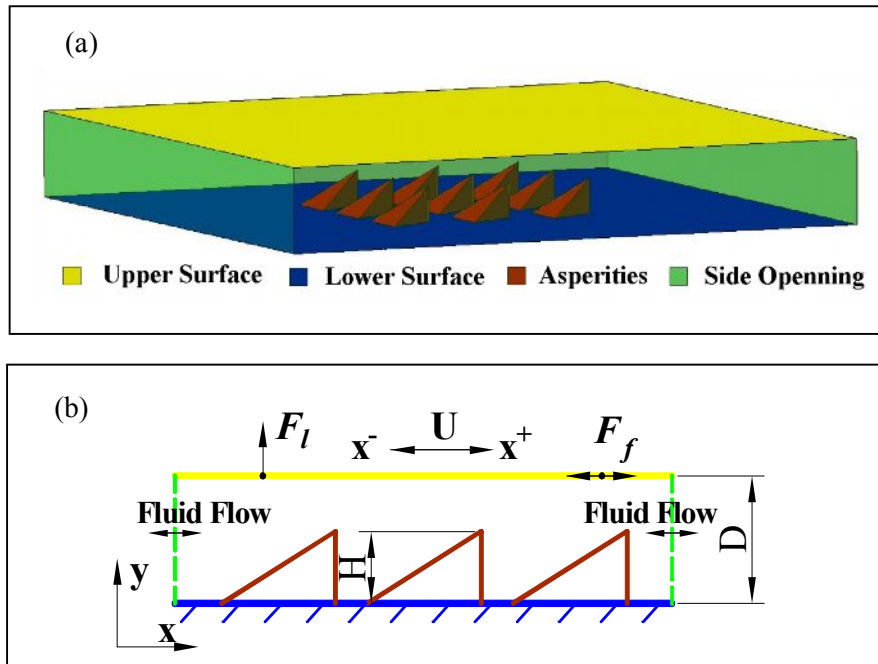
Fig. 3.1 General geometry for the friction model: (a) perspective view and (b) side view

The distance between the two surfaces is fixed (i.e. the upper surface cannot move up and down with respect to the stationary lower surface), and the distance is denoted by D (D is measured from the bottom of the lower surface, as shown in Fig. 3.1b). The height of the asperity is denoted by H (Fig. 3.1b). In this research, the height H is randomly chosen, but it follows the definition of the micro asperity discussed in section 1.1.3. The distance between two surfaces, D, is chosen to have the same order of magnitude as the asperity height. If D is too large, the effect of the asperities on friction force would be too slight to make sense. If D is too small, friction is in a boundary or mixed friction state, and is beyond the scope of this thesis.

When the upper surface travels along the +x or the −x direction, there will be a friction force F_f^+ or F_f^- on it. The movement of the upper surface will cause the hydrodynamic effect because of a series of wedged gaps between the two surfaces. The hydrodynamic effect (i.e., pressure) will then generate a lifting force F_l on the upper surface (Fig. 3.1b). The objective of modeling is to establish a model with which to compute the friction force F_f and lifting force F_l, respectively.

The above problem can be categorized as a fluid flow problem in fluid mechanics, and it can also be considered as a lubrication problem in tribology. This research considers the problem as a fluid mechanics problem, and further, the CFD technique will be employed to solve this fluid mechanics problem. In the CFD modeling, important steps include: making proper assumptions for the problem, selecting governing equations, and determining boundary conditions. The subsequent sections will discuss these steps in detail.

3.3 Assumptions

The model to be established will be based on the following assumptions:

Assumption (1): The flow is laminar flow. The Reynolds number $Re = \rho U L/\mu$ (L is the characteristic length of the fluid domain, ρ is the density of the lubricant, U is the speed of the upper surface, μ is the viscosity of the lubricant) will always be smaller than 100 in all concerned configurations. If $Re = 100 < 1000 < 2000$, the flow is a laminar flow ($Re = 1000$ is considered as a value that the flow in the pipe has very less possibility of becoming a turbulent flow, while $Re = 2000$ is considered as a value that the flow in the pipe usually starts to become turbulent. The situation for the flow in the pipe is also applicable to the flow dealt with in this thesis).

Assumption (2): The flow is incompressible Newtonian flow. It is noted that in this study, a lubricant which shows a strong Newtonian flow behavior is considered.

Assumption (3): The lubricant will not slip on the solid surface. It is noted that there will always be some slip between the lubricant fluid and its boundary surface; the key is the degree of slip. The degree of slip further depends on the degree of hydrophobic of the solid surface with respect to the lubricant. The less hydrophobic the solid surface is, the less slipping of the lubricant will occur on the surface. In this study, the hydrophobic property of the solid surface is considered to be minimal, so a non-slip condition is reasonable.

Assumption (4): The flow is fully developed and in a steady state. When the upper surface starts to move, only a layer of the lubricant which is closest to the upper surface will start to

move. After a certain period, all of the lubricants (except that closest to the stationary surface) within the domain will move, the movement of the lubricant comes to a dynamically balanced state. In this state, ideally, at each point within the fluid domain, the properties of the flow will not change with respect to time. The force on the solid surface will not change as well. This state is called fully developed and steady state, and this thesis considers the fluid to be in such a state only. That is to say, the flow of lubricant, its properties (e.g., velocity, pressure) will not change with respect to time at any point between the upper surface and lower surface, as well as the lifting force and friction force on the upper surface.

Assumption (5): The pressure (gauge pressure) of the fluid at the openings is zero. This means that there is no external pressure (negative or positive) to push or pull the fluid at the openings.

Assumption (6): Gravity force is the only external force acting on the fluid, and it is negligible. External forces are the forces that come from the fluid mass (for example, the gravity forces, magnetic forces, centrifugal forces if the fluid is contained inside a rotational container). The magnitude of the external force usually depends on the mass of the fluid. In this study, it is assumed that the fluid flows in an environment without any external force except gravity; furthermore, as the mass of the fluid is very small, the gravity force applied on the fluid is therefore negligible.

3.4 Governing Equation

In the literature on lubrication modeling, the Reynolds equation is frequently used, because it is simple and applier very well to the situation of bearing lubrication. However, in the literature on fluid dynamics, the Navier-Stokes (NS) equation is frequently used, because it introduces the least number of assumptions and it is for the most general situation of fluid dynamics (e.g., those with turbulence or those with complex structures). From the literature review presented in section 2.4, it can also be seen that the Reynolds equation and the NS equation are two major equations for modeling the inter-asperity flow.

The Reynolds equation can be derived from the NS equation with some additional assumptions. These additional assumptions are: a) the pressure across the fluid thickness does not change (constant pressure assumption); b) the inertia force acting on the fluid is very small or negligible compared to the viscous force (negligible inertial force assumption); and c) the rate of change of the velocity along any direction other than film thickness direction is very small or negligible (constant velocity assumption) [Hori, 2006]. The following shows the Reynolds equation with two dimensions [Hori, 2006], where, U and V are the horizontal speeds (along x-direction) and vertical speed (along y-direction or film thickness direction) of the upper surface, respectively.

$$\frac{\partial}{\partial x}\left(h^3 \frac{\partial p}{\partial x}\right) + \frac{\partial}{\partial z}\left(h^3 \frac{\partial p}{\partial z}\right) = 6\mu\left(U \frac{\partial h}{\partial x} + 2V\right) \qquad (1)$$

Satisfying the first assumption (i.e., constant pressure assumption) inherently requires that the surface should be very "smooth" if the thickness of the lubricant films is relatively small. This is called the smooth surface requirement here. The word "smooth" means that the change of the

surface height along the flow direction is not great. In other words, if L_y is the asperity height and L_x is the asperity length; then $L_y/L_x \ll 1$ (see Fig. 3.2 for a visual impression). The statement "The lubricant film is relatively small" means that the difference between the film thickness and the height of the asperity is not great and they are on the same order of magnitude; i.e. if D is the film thickness, $L_y/D \approx 1$. Fig. 3.2 further illustrates the concept of "smooth" with two situations where there is a lubricant film with a small thickness: in the first case, the lower surface is considered as a smooth surface because it meets the requirement of the first assumption, but the second case does not. If the surface is not smooth, as it will be shown in later simulations, the pressure will change across the film thickness.
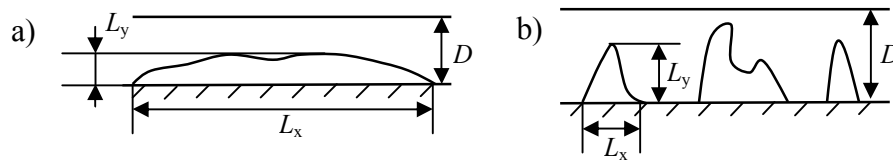
Fig. 3.2 a) Surface is smooth (where $L_y/L_x \ll 1$, $L_y/D \approx 1$)
b) Surface is not smooth (where $L_y/L_x \approx 1$, $L_y/D \approx 1$).

Satisfying the second assumption (i.e., negligible inertial force assumption) inherently requires that the smooth surface requirement is satisfied or the flow has a low Reynolds number (less than 1). This is called the low Reynolds number requirement here.

Satisfying the third assumption (constant velocity assumption) inherently requires that the change of the geometry of the surface should be very smooth along any direction other than the film thickness direction, particularly the z-direction (other than x- and y- direction shown in Fig. 3.1). This is called smooth z-direction geometry requirement.

If the low Reynolds number requirement can be satisfied, the second assumption (i.e., negligible inertial force assumption) will be directly satisfied from first principles. If the smooth surface requirement can be satisfied, the inertial effect on the surface can be avoided, as the smooth surface has fewer blockages on the lubricant fluid, so the inertial of the lubricant fluid has less chance to be transferred to the force acting on the solid surface. In this case, the negligible inertial force assumption is indirectly satisfied.

In this study, none of the smooth surface requirement, low Reynolds number requirement and the smooth z-direction geometry requirement will be satisfied. Fig. 3.3 shows one of the configurations the model will be applied to (details of the configuration can be found in chapter 5). From this figure it can be seen that the asperity height $H = 5\mu m$ (which corresponds to L_y); the distance between the two surfaces $D = 7.5\mu m$, the asperity width $c = 10\mu m$ which corresponds to L_x. Therefore L_y/D equals 0.667 which indicates that the film thickness is relatively small, and $L_y/L_x = 0.5 \approx 1$ but not $\ll 1$ which indicates the surface is not smooth. Therefore, the smooth surface requirement is not satisfied. Fig. 3.3 also shows that the asperities and the gaps in-between form sharp geometry changes along the non-thickness-direction. Therefore, the smooth z-direction geometry requirement is not satisfied. It can also be seen from Fig. 3.3 that the Reynolds number $Re=\rho Ul/\mu=900$ (kg/m^3) $\times$ 2 (m/s) $\times$ 4.5$\times$10^{-5} (m) / 0.04(Pa s) = 2.025 (l is the characteristic length of the surface, and it equals 45μm). This suggests that the low Reynolds number requirement is not satisfied, as the Reynolds number is still larger than 1 (though quite small).

H=5 μm
D=7.5 μm
c=10 μm
ρ=900 kg/m^3
U=2 m/s
l= 45μm
μ=0.04 Pa s
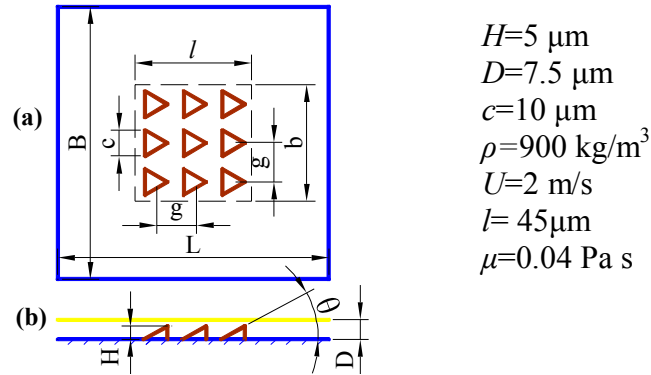
Fig. 3.3 One of the configurations the developed model will be applied on

From the above discussion, it can be seen that the Reynolds equation is not applicable to the problem in this study as its assumptions cannot be satisfied. The NS equation has to be used as the governing equation.

3.5 Boundary Conditions

The boundary conditions (BCs) are another important aspect of model development. There are BCs on the solid surface (including the upper surface, lower surface and the asperity surface) and BCs on the side openings (see Fig. 3.1a).

On the solid surfaces, the non-slip condition is used based upon the assumption (3). The fluid in contact with the solid surface has the same velocity as the solid surface. That is to say, for the lubricant fluid in contact with the lower surface and asperity surface, its velocity is zero. For the lubricant fluid in contact with the upper surface, its velocity tends to be the same as the upper surface which is in moving at speed U.

On the side openings, the pressure is zero based on assumption (5). There is no external energy to drive the flow. In an initial state, the velocity on the side openings tends to zero. The energy that causes the flow comes from the movement of the upper surface. The fluid is brought into or out of the fluid domain by the dragging force of the upper surface.

Beside the two BCs discussed above, there is one more important BC, that is the BC for the film ruptured area or cavitation area. As previously discussed in the literature review in section 2.4, if the NS equation is selected as a governing equation, the density based cavitation model or the multi-phase simulation model may be employed. They need some other information, e.g., density function, which is not readily available in the problem considered in this thesis, so restricting their use for our problem. If the Reynolds equation is used as a governing equation, the Reynolds condition only tells where the cavitation area starts (i.e., where the pressure gradient is zero), but it cannot tell where the cavitation area ends. Therefore, the Reynolds condition is not applicable to the problem where the cavitation occurs within the fluid flow. It is further noted that the JFO model is developed based on the Reynolds condition [Schweizer, 2009], and it can tell where the cavitation ends (at the locus where the pressure resumes). However, the JFO model is not suitable to our problem.

In this study, the Half-Sommerfeld Condition (HSC) will be employed with the NS equation. This could be the first time that these two models are used together. The Half-Sommerfeld condition (Gümbel's boundary condition as it is called in some literature) was proposed by Gümbel in 1921. The HSC considers the area where the pressure is smaller than the ambient pressure (usually 0 Pa, gauge pressure) as the cavitation area. Here, the pressure is the

"preliminary" pressure which is known by solving the NS equation or Reynolds equation. Within this area, the pressure will be maintained at a saturation level which is similar to the ambient level [Hamrock and Schmid, 2004]. It is assumed that the area where the pressure is less than the ambient pressure will be dominated by gas (i.e., the air dissolved in the lubricant), and it is the gas that maintains the pressure in these areas at a particular saturation level. In this study, the HSC is used in such a way that in the area where the pressure is less than the ambient pressure, the pressure in this area will be set back to the ambient pressure.

Further, the area where the pressure is less than the ambient pressure is called **film ruptured area** in this thesis for the convenience of later discussions. It is further assumed that the drag from the film ruptured area on the upper surface is negligible (if the film ruptured area is close to or on the upper surface) compared with that from the non-ruptured area. This is because the drag of the fluid on the moving surface depends on the viscosity of the fluid. The larger the viscosity is, the larger the drag will be. The film ruptured area is dominated by gas, while the non-ruptured area is dominated by the liquid lubricant, and the viscosity of the gas is far less than that of liquid lubricant.

In short, the non-slip condition will be used for the solid surfaces; the zero ambient pressure (i.e., the ambient pressure is equal to one atmosphere pressure, it is measured in gauge pressure) will be used for the side openings; the HSC will be used for the film ruptured area; and the drag from the film ruptured area on the upper surface is negligible.

3.6 Mathematical Expression of the Model

The following is a list of the mathematical expressions of the model. Equations (2) and (3) are the NS equation and continuity equation, respectively. They are applicable to the situation where the flow is laminar and incompressible, with respect to Assumption (2) and (3). The time variant term and source term are neglected based on Assumption (5) and Assumption (7). Equation (4) is a mathematical expression of the boundary condition for the solid walls and side opening. For the BC of side openings in Equation (4), it is determined based on Assumption (6) – zero ambient pressure. For the BC of the upper and the lower surfaces, it is determined with respect to Assumption (4) – non-slip condition. Particularly, $y=\Phi(x, z)$ describes the geometry of the lower surface. For the regular asperity surface, the $\Phi(x, z)$ can be determined without using any statistical method. From equations (2-4), the "preliminary" pressure distribution within the fluid domain including that on the upper surface $p(x, y, z)$ can be calculated, and so can the velocity distribution $u(x, y, z)$ in the x-direction. From $u(x, y, z)$, the gradient of the velocity u along the y-direction du/dy can be determined.

$$\rho\left(u\frac{\partial u}{\partial x}+v\frac{\partial u}{\partial y}+w\frac{\partial u}{\partial z}\right)=-\frac{\partial p}{\partial x}+\mu\left(\frac{\partial^2 u}{\partial x^2}+\frac{\partial^2 u}{\partial y^2}+\frac{\partial^2 u}{\partial z^2}\right)$$

$$\rho\left(u\frac{\partial v}{\partial x}+v\frac{\partial v}{\partial y}+w\frac{\partial v}{\partial z}\right)=-\frac{\partial p}{\partial y}+\mu\left(\frac{\partial^2 v}{\partial x^2}+\frac{\partial^2 v}{\partial y^2}+\frac{\partial^2 v}{\partial z^2}\right) \tag{2}$$

$$\rho\left(u\frac{\partial w}{\partial x}+v\frac{\partial w}{\partial y}+w\frac{\partial w}{\partial z}\right)=-\frac{\partial p}{\partial z}+\mu\left(\frac{\partial^2 w}{\partial x^2}+\frac{\partial^2 w}{\partial y^2}+\frac{\partial^2 w}{\partial z^2}\right)$$

$$\frac{\partial u}{\partial x}+\frac{\partial v}{\partial y}+\frac{\partial w}{\partial z}=0 \tag{3}$$

$$\begin{cases} \text{Side openings} & p(x,y,z)=0 \\ \text{Upper surface} & u(x,y,z)=U, v(x,y,z)=0, w(x,y,z)=0 \\ \text{Lower suface} & u(x,y,z)=0, v(x,y,z)=0, w(x,y,z)=0 \end{cases} \tag{4}$$

$$P(x,y,z) = \begin{cases} 0 & p(x,y,z) < 0 \\ p(x,y,z) & p(x,y,z) \geq 0 \end{cases} \tag{5}$$

$$a(x,y,z) = \begin{cases} 0 & p(x,y,z) < 0 \\ 1 & p(x,y,z) \geq 0 \end{cases} \tag{6}$$

$$k = \frac{1}{bl} \int_0^b \int_0^l a(x,y,z)\Big|_{x,D,z} \, dxdz \tag{7}$$

Further, equation (5) shows the application of the HSC. $P(x, y, z)$ is the pressure distribution within the fluid domain after the application of the HSC. Equations (6) and (7) show the calculation of the percentage of the area on the upper surface with positive gauge pressure. This will be used to accumulate friction force only from the drag produced in the non-film-ruptured area. Equation (8) shows the calculation of friction force on the upper surface. This equation is established based on the law of the Newtonian fluid – the shear stress is proportional to the shear rate of the fluid. The friction force is calculated by integrating the shear stress on the upper surface over the whole upper surface, where the pressure is larger than the ambient level (i.e., the non-film-ruptured area). This is done by integrating the shear rate over the whole upper surface and then multiplying it with the lubricant dynamic viscosity μ and the percentage k, namely

$$F_f = k\mu \int_0^b \int_0^l \frac{du(x,y,z)}{dy}\Big|_{x,D,z} \, dxdz \tag{8}$$

$$F_l = \int_0^b \int_0^l P(x,y,z)\Big|_{x,D,z} \, dxdz \tag{9}$$

Equation (9) shows the calculation of the lifting force on the upper surface, and it equals the integration of the pressure distribution on the upper surface over the entire upper surface area.

In the above, eight equations need to be solved, and two of them are partial differential equations (PDF). A numerical method which is based on the finite volume method (FVM) will be used to solve these equations, and furthermore, the commercial CFD software will be used for the FVM implementation.

3.7 Summary

Thus far, it is possible to calculate lifting force and friction force on the upper surface with the model developed. The friction coefficient, conventionally for the irregular asperity surface, may be calculated by dividing the lifting force by friction force. Fig. 3.4 summarizes the procedure for solving the model to obtain friction force and lifting force.
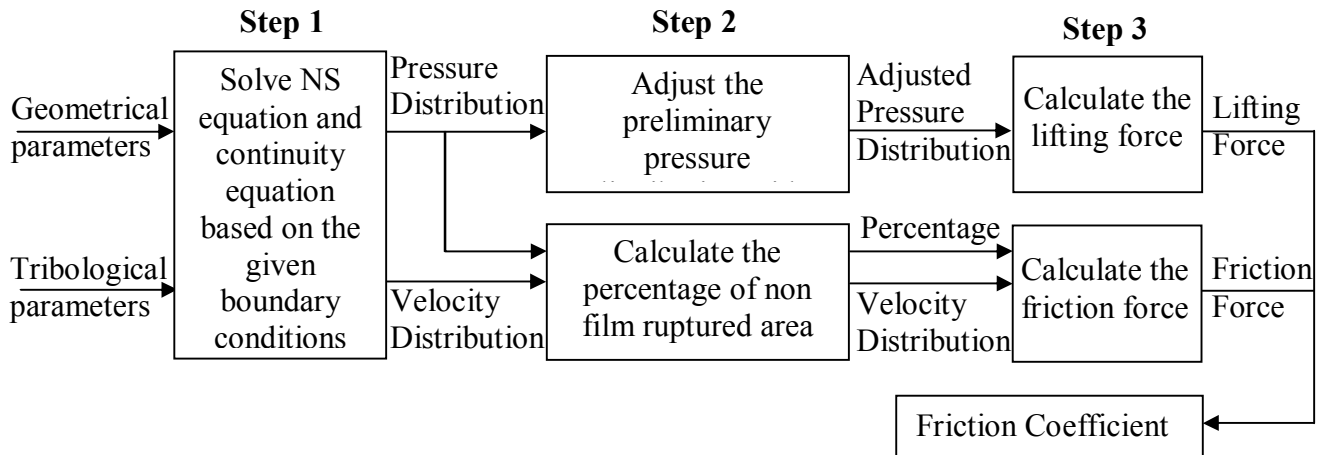
Fig. 3.4 Procedures for solving the model to obtain lifting force and friction force

CHAPTER 4 MODEL VERIFICATION

4.1 Introduction

Though the model developed in chapter 3 is specifically for a surface with anisotropic asperities, it is also applicable to a surface with isotropic asperities. In this chapter the model developed in chapter 3 (called "NS-HSC Model" for short in the following text, as the NS equations and HSC are used in the model) will be verified using a surface with regular isotropic asperity because of the availability of experimental results in the literature. The general idea of the verification is to compare the result predicted by the NS-HSC Model and the result acquired from experiment and other existing models reported in [Stephens et al., 2004]. The following will first give a brief introduction of the experimental process and the result presented in [Stephens et al., 2004], followed by a brief introduction of the calculation process and the result generated with the model presented in [Stephens et al., 2004] (called "RE-HSC Model" in the following text, as the Reynolds equation and the HSC are used in the model) and the NS-HSC Model. Comparison of the three results would verify the effectiveness of the NS-HSC Model. At the end of this chapter, a discussion will be presented to explain the reason why the NS-HSC Model predicts a result closer to the experimental result than the existing model of [Stephens et al., 2004].

4.2 Results of the RE-HSC Model and Experiment

Fig. 4.1 shows the test rig in [Stephens et al., 2004]. There are two rings in the test rig (Fig. 4.1a). On the surface of the lower ring, there are RIAs with a hexagonal shape and hexagonal distribution pattern (Fig. 4.1b). The surface of the upper ring is flat. The specific size of the surface is as follows: the outer diameter and the inner diameter of the ring are 28.6mm and 25.4mm, respectively; the height and the diameter of the asperities are 1-100μm and 550μm, respectively; the edge to edge distance between two asperities is 165μm.
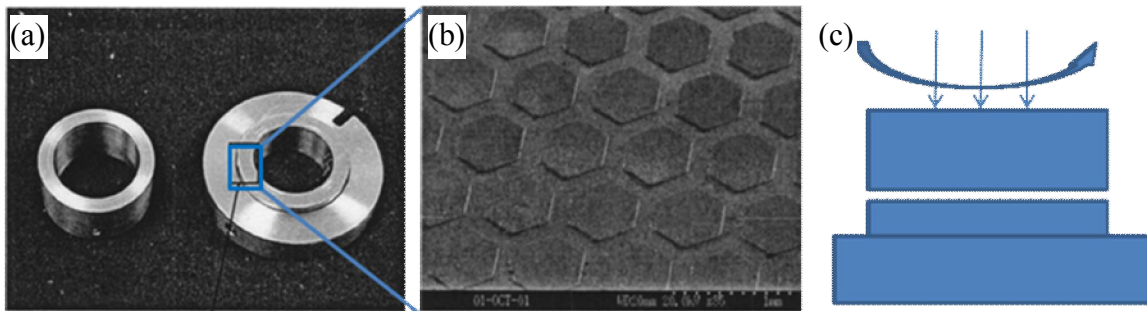
Fig. 4.1 Surface and test rig introduced in [Stephens et al., 2004]

During the test, the upper ring rotates with respect to the lower ring (Fig. 4.1c). The upper ring is subject to a constant load ($0.1N/mm^2$), and there is a lubricant supply between the two rings. Different lower rings with asperities of different heights are used in the test. The distance between the two surfaces when they come to a steady state is measured as well as the torque to drive the upper ring to rotate at 2500 RPM (surface velocity of 3.5m/s). The friction force on the upper ring is calculated by dividing the torque with the average radius of the upper ring. The friction coefficient was calculated by dividing the friction force by the load (i.e., the lifting force). Table 4.1 lists the result for the case with asperity heights of 7 and 14 μm, respectively.

The RE-HSC model was based on a simplified geometry. It takes part of the lower surface named *unit cell*. Each unit cell has one hexagonal asperity and its surrounding space. The hexagonal asperity is further approximated into a cylindrical asperity, so does the original hexagonal unit cell (Fig. 4.2). The geometrical parameters of the unit cell are shown in Fig. 4.2 as well as the tribological parameters for the test. These parameters are the same as the parameters of the sample used in the experiment. The governing equation for the RE-HSC model is the Reynolds equation, and HSC was used for the film ruptured area. The result calculated with this model is also listed in Table 4.1.

$R=357\mu m$
$r = 275\mu m$
$H = 7$and 14 μm
$U=3.5m/s$
$\rho=900kg/m^3$
$\mu=0.102Pa\ s$
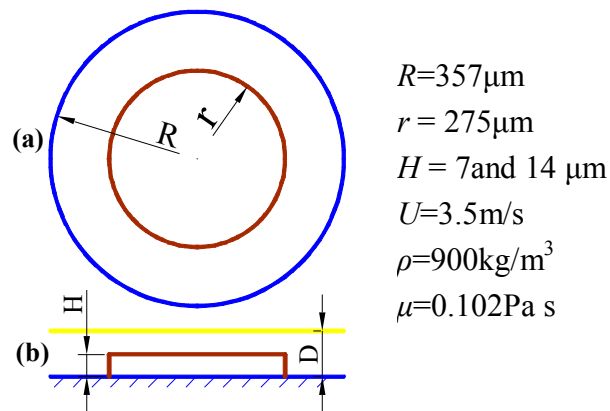
Fig. 4.2 Geometry of a Unit Cell and its parameters

4.3 Results of the NS-HSC Model

In this chapter, the NS-HSC Model will be tested on the same configuration as the RE-HSC Model; see Fig. 4.2. The same configuration means both the geometrical and tribological parameters are the same. However, the NS equation is used as the governing equation in the NS-

HSC Model, as opposed to the Reynolds equation used as a governing equation in the RE-HSC Model. The HSC is used in both models. The implementation of the NS-HSC Model and solution process of the NS-HSC Model are implemented with the help of commercial software, and the following shows the specific steps:

(1) The geometry of the lower surface as well as the upper surface and the fluid domain is established in the commercial CAD software *SolidWorks*.

(2) The fluid domain is discretized with the commercial CFD software *ANSYS ICEM* 11.0. About one million 3D unstructured tetrahedron meshes are used to mesh the cylindrical domain, whose diameter is 714 microns and height is less than 20 microns. At the sharp edges of the top surface of the asperity, the meshes are densified to improve the continuity of flow with respect to the mass and the momentum during the mathematical solution process (Fig. 4.3).

The meshes on the surface of the asperity top

The meshes on the surface of the asperity side

The meshes on the base of the lower surface
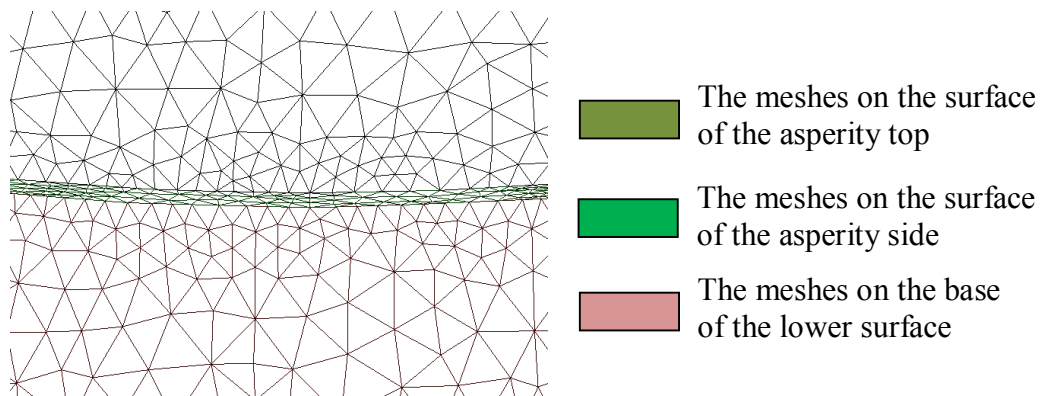
Fig. 4.3 Densified unstructured mesh near the sharp edge of the asperity

(3) The solution of the equations presented in section 3.6 is conducted with *ANSYS FLUENT*

12.0. The properties of the fluid and the boundary conditions listed in equation (4) and Fig. 4.2 are specified in the pre-solution process of *ANSYS FLUENT 12.0.* The 3D laminar pressure based solver for steady state calculation is used for solving the NS equation and continuity equation in the NS-HSC Model. The first-order upwind scheme is used for the solution. When the residuals of continuity, the xyz-direction velocities are all below 10^{-3}, the solution is considered converged. Fig. 4.4a shows the pressure distribution on the upper surface before the HSC adjustment.

(4) The HSC implementation and the calculation of the percentage of non-film-ruptured area are conducted with the help of user defined functions. The CFD software itself does not provide an option to implement the HSC directly. This is done by defining a user defined function (UDF, it is an interface provided by *ANSYS FLUENT 12.0* to satisfy users' additional calculation requirements), and this is taken in this study. The UDF for the HSC implementation and percentage calculation is listed in Appendix A. Fig. 4.4b shows the pressure distribution on the upper surface after the HSC adjustment;

(5) Friction force and lifting force are calculated. The results form *ANSYS FLUENT 12.0* include lifting force, but not friction force. Friction force is calculated by multiplying the percentage value calculated in step (4) with the "preliminary" friction force obtained from *ANSYS FLUENT 12.0.*

With the five steps above, lifting force and friction force can be obtained. A trial is made to determine the distance between the upper and lower surfaces (*D* in Fig. 4.2) so that the lifting

force on the upper surface can reach 0.0402N (i.e. 0.1N/mm^2, the same as in the experiment) for each case, and the friction coefficient is also calculated with the trial D. The results including the friction coefficient and the distance D are listed in Table 4.1.
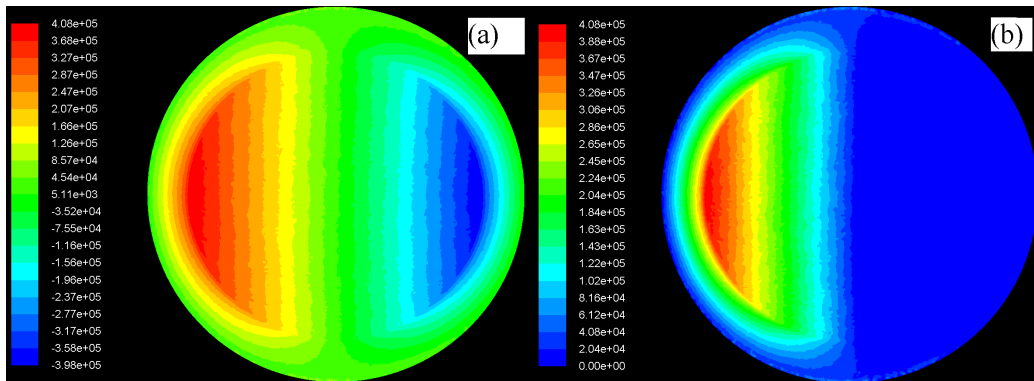
Fig. 4.4 Pressure distribution on the upper surface (a) before and (b) after the implementation of HSC

4.4 Results and Discussion

Table 4.1 lists the experimental result of [Stephens et al., 2004] and the result obtained from the RE-HSC Model, as well as the result predicted by the NS-HSC Model. From Table 4.1, the following observations can be made:

Observation (1): The friction coefficient predicted by the NS-HSC Model is closer to the experimental result than that predicted by the RE-HSC Model for both the 7 and 14 μm cases.

Observation (2): The difference of the friction coefficient between the experimental result of [Stephens et al., 2004] and the predicted result with the NS-HSC Model is 16.7% for

the 7μm case and 33.3% for the 14 μm case.

Table 4.1: Tribological results from the experiment, RE-HSC and NS-HSC models

| Asperity Height | Result from literature [Stephens et al., 2004] | | | | Result from NS-HSC Model | |
| | Experimental | | Theoretical | | | |
	Distance btw. surfaces	Friction coefficient	Distance btw. Surfaces	Friction coefficient	Distance btw. surfaces	Friction coefficient
7 μm	16.7μm	0.30	14.8μm	0.37	14.8μm	0.36
14 μm	22.1μm	0.32	18.8μm	0.52	19.4μm	0.48

* Based on the same lifting force/load at 0.1N/mm^2 on the upper surface

Observation (3): The friction force predicted by the NS-HSC Model is smaller than that predicted by the RE-HSC Model.

Observation (4): For the 7 μm case, the distance predicted by the NS-HSC Model is 14.8 μm which is the same as the RE-HSC Model, but for the 14 μm case, the NS-HSC Model predicts a distance which is closer to the experimental result.

From Observation (1), it can be concluded that the NS-HSC Model is better than the RE-HSC Model. The reason is because in the RE-HSC Model, the friction force is calculated over an entire upper surface area without considering the effect from the film-ruptured area. As discussed before, in the area where there is a film rupture, the friction force is quite small and nearly zero

due to the small viscosity of the dominant gas within the film-ruptured area. That is why the NS-HSC Model predicts a more accurate and smaller friction coefficient result than the RE-HSC Model, i.e. Observation (1) and (3). This further supports the notion of the film ruptured area as well as the proposed approach to modeling friction force in such an area.

Observation (2) tells that there are 16.7% and 33% difference of the friction coefficient between the result predicted by the NS-HSC Model and the experimental result. This difference comes mainly from the physical difference between the test rig and the configuration the NS-HSC model based on (Fig. 4.2). The use of the HSC may also lead to the difference between the results. This is because the HSC will bias the theoretical result from the experimental result as the application of the HSC is applied after the NS equation, which does not capture the real physics of the fluid, as in real situations, fluids in the film ruptured area and in the non-film ruptured area behave at the same time under all boundary conditions. The physical difference between the test rig and the configuration the HS-HSC model is based on includes: a) the simplification of the geometry from the whole surface on the ring in the experiment to a unit cell considered in the application of NS-HSC Model; b) the change of the lubricant property due to the temperature drifting in the experiment is neglected in the NS-HSC Model; c) the change of the form of the motion from the rotation in the experiment to the translation in the NS-HSC model. Never the less, the results obtained from the NS-HSC Model still largely capture the effect of the regular asperity on friction force, and the model is still applicable to the study of directional friction on a fully lubricated surface. Besides, the NS-HSC Model and the RE-HSC Model were based on the same configuration (i.e., all the parameters, geometrical, dynamical and tribological, are the same, except distance *D*). Therefore, the conclusion from Observation (1)

(i.e., the NS-HSC Model is better than the RE-HSC model) is valid and sound.

For Observation (4), it is because the RE-HSC Model is based on the Reynolds equation, and the Reynolds equation is based on the smooth surface assumption as mentioned in section 3.4. Here, the surface with 14 μm asperities is less smooth than the surface with 7 μm asperities, so the result predicted by the RE-HSC Model is less accurate for the 14 μm cases. This degradation in accuracy is not evident in the result of the NS-HSC Model. This is further evidence to support the use of the NS equation for modeling the problem in this study.

4.5 Conclusion

In this chapter, based on the same geometry, the result predicted by the NS-HSC Model was compared with the experimental result and the result from the RE-HSC Model. It has been found that the NS-HSC Model predicts a result that is closer to the experimental result than the RE-HSC Model. It has also been found that the predicted distance between the two surfaces deviates further from the experimental result of [Stephens et al., 2004] with the RE-HSC Model than the NS-HSC Model. An analysis has been given to explain the results, and it can be concluded that: (a) the film ruptured area needs to be considered and modeled for the problem in this study; (b) the Reynolds equation is not suitable to the problem in this study; (c) the NS-HSC Model is applicable to the study of directional friction on a fully lubricated RAA surface.

However, there are some limitations with the NS-HSC Model, and they are: (a) there is a discrepancy larger than 10% between the result predicted by the NS-HSC Model and the experimental result; and (b) the application of the HSC is after the computation with the NS

model, which contributes to the deviation of the NS-HSC Model from the physical reality. These limitations will be overcome in the future study by refining the experimental setups, and using more sophisticate models for the film ruptured area, for example the density based cavitation model discussed in [Brajdic-Mitidieri et al., 2005] or a multiphase flow model.

CHAPTER 5 DIRECTIONAL FRICTION

5.1 Introduction

In this chapter, the NS-HSC Model developed and verified in the preceding chapters will be applied to two surfaces with regular anisotropic asperities, in particular one RAA surface of square cross-section and the other RAA surface of triangular cross-section. Friction force on the upper surface will be computed to examine whether directional friction is evident. A comparison will then be given to study how the shape of the asperity would affect directional friction (if it is presented). At the end of this chapter, a discussion will be given to explain the reason why directional friction is feasible or why not. Phenomena observed in the comparison will be discussed as well.

5.2 Configuration of RAA Surfaces

Two configurations of surfaces with RAAs are presented in Fig. 5.1. Fig. 5.1a shows the surface with RAAs that have triangular cross-section (from top view), and Fig. 5.1b shows the surface with RAAs that have square cross-section (from top view). The two surfaces have an array of asperities. The details of the surface geometry are shown in Table 5.1.
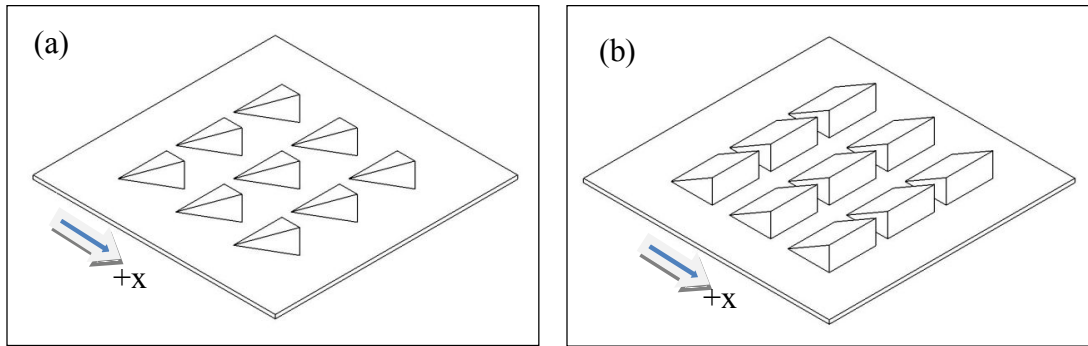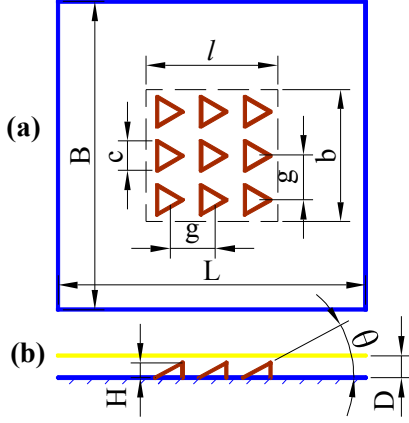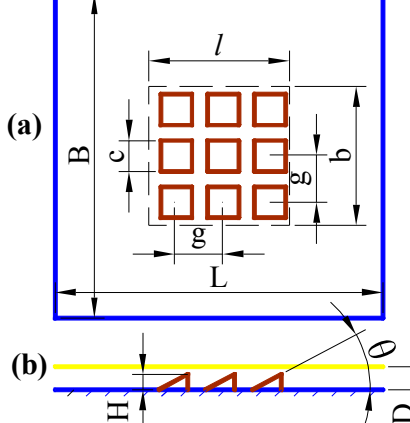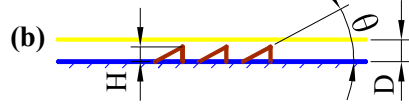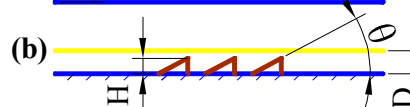
Fig. 5.1 Surfaces with RAAs that have (a) triangular cross-section and (b) square cross-section

It can be further seen from Fig. 5.1 that along the direction of arrow (i.e., the +x direction), the geometry of the asperities on both surfaces experience a positive gradient in height (i.e., the height of the asperities is increasing along the +x direction). However, for the RAAs with triangular cross-section (triangular asperity for short in the following text), they experience a negative gradient in width at the same time (i.e., the width of the asperities reduces along the +x direction).

The structure of the RAA surfaces of Fig. 5.1 can further imply the following behaviors of flows of fluid: (1) there will be less blockage on fluid if the fluid flows along the +x direction for both the triangular and square asperities; (2) There will be fewer blockages on fluid with the triangular asperity than that with the square asperity if the fluid flows along the -x direction; (3) There will be more differences in blockage of the fluid between the two opposite directions (+, -) with the square asperity than that with the triangular asperity.

Table 5.1: Configurations of friction structure and their parameters

Configuration 1: triangular asperities			Configuration 2: square asperities	
$B=L=105\mu m$	$D=7.5\mu m$	$g=15\mu m$		$\mu=0.04Pa\ s$
			$U=2m/s$	
$b=l=45\mu m$	$H=5\mu m$	$c=10\mu m$		$\rho=900kg/m^3$

* (a) Top view without upper surface, x-z plane; (b) Side view with upper surface, x-y plane;

** The colors in the figure have the same indication as those in Fig. 3.1.

In Table 5.1, it is noted that the asperity in Configuration 2 (square asperity) is designed for the purpose of making a comparison with Configuration 1 to understand how the geometry of the asperity affects the directional friction behavior. Further, the parameters in these two configurations have the same value, and they are arbitrary. It is worth mentioning that the surface area ($B\times L$) used in the two configurations is designed to be larger than the area where the asperity actually takes ($b\times l$), and this is for the purpose of eliminating potential disturbances coming from the edges of the upper surfaces at the side openings. These disturbances could come from the mathematical processes during the solution of the NS-HSC model. This study will only focus on the area within ($b\times l$).

5.3 Application of the NS-HSC Model

The NS-HSC model is applied to the sample surfaces with triangular RAAs and square RAAs, respectively, based on the similar steps presented in section 4.3. Commercial CAD and CFD software systems are employed to build up the computational model. The geometry of the structure is established in the CAD software system. The domain of fluid flow is discretized into about two million unstructured tetrahedron meshes with the meshes at sharp edges being further densified (Fig. 5.2). The parameters of traveling speed of the upper surface, properties of the fluid, and boundary conditions on the mesh are specified with *ANSYS FLUENT 11.0*. The steady sate incompressible laminar flow solver is employed for solving the model. The first-order upwind scheme is selected to discretize the NS equation. After about 120 iterations, the solution is considered converged and a preliminary pressure distribution is obtained (Fig. 5.3a). The HSC is then applied with the UDF, the percentage of non-film-ruptured area is calculated, and the pressure distribution is adjusted (Fig. 5.3b). Finally, friction force and lifting force are calculated. For each case, triangular or square, the NS-HSC model is applied twice to calculate the friction force on the upper surface when it moves along the two opposite directions (i.e., the +x and the − x directions). The final result of the friction force is given in Table 5.2 in the next section.
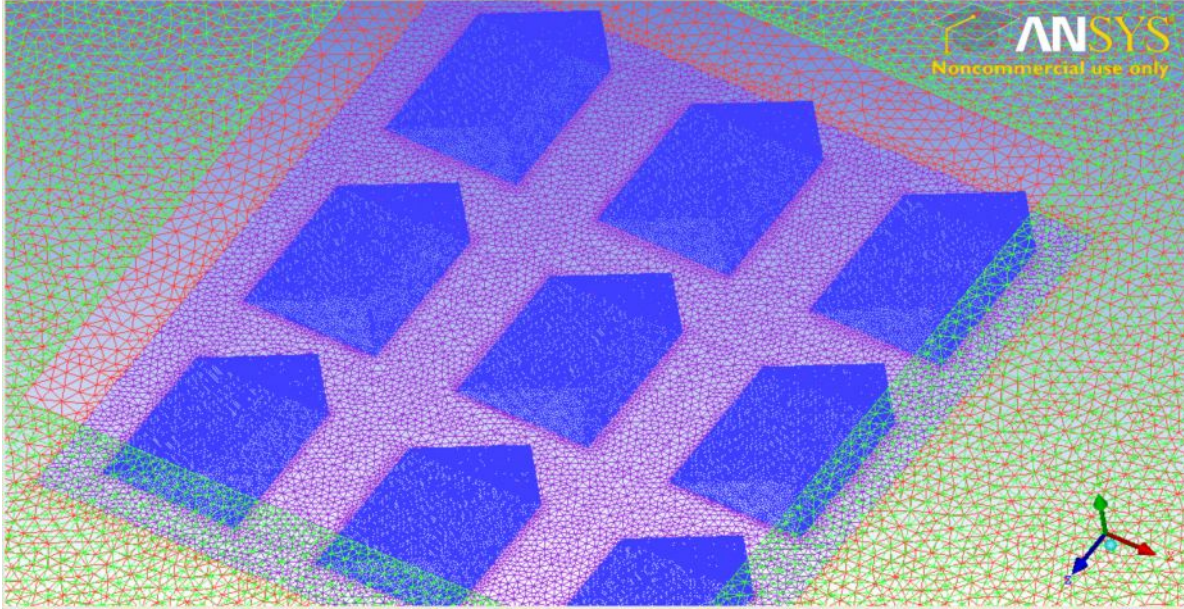
Fig. 5.2 Tetrahedron meshes that discretized the flow domain
(Red meshes – these are close to the lower surface outside of $b{\times}l$ area; Purple
meshes – these are close to the lower surface within $b{\times}l$ area; Blue meshes – these
are on the asperities; Green meshes – these are close to the upper surface outside of
$b{\times}l$ area; the area on the upper surface within $b{\times}l$ is not displayed here)
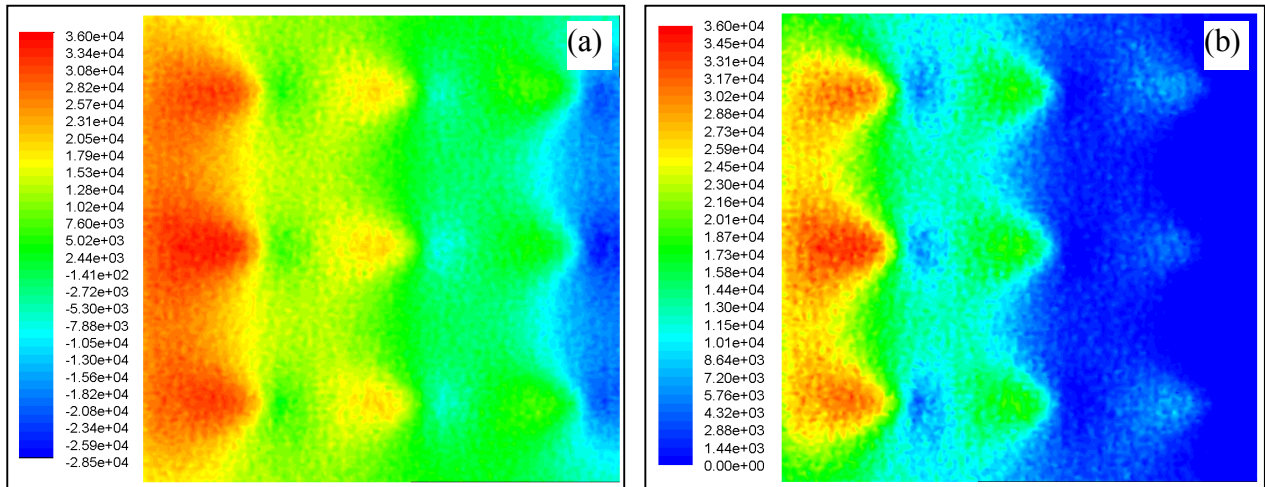
Fig. 5.3 Pressure distribution on the upper surface when it travels towards the +x direction
above the triangular RAA surface (a) before HSC adjustment; (b) after HSC adjustment

5.4 Results

Table 5.2 shows the friction force on the upper surface when the upper surface moves along the two opposite directions (+x, -x) on the fully lubricated surface with the triangular or square RAAs. From Table 5.2, three phenomena can be observed:

Table 5.2: Friction force calculated with different asperities and directions ($\times 10^{-5}$N)

Direction	Triangular RAA	Square RAA
+x	2.75	3.06
-x	2.36	1.73

Phenomenon 1: The friction force is different with respect to the two opposite directions of travel for both the triangular and square asperities. This means that directional friction is written on the fully lubricated surface with regular anisotropic asperities.

Phenomenon 2: In the both cases, the friction force is larger when the upper surface moves along the +x direction than when it moves along the –x direction. Here the +x direction means the direction along which the upper surface will push the fluid into a convergent gap (Fig. 5.4a, c). The –x direction means the direction along which the upper surface will drag the fluid out of the convergent gap (Fig. 5.4b, d). This phenomenon somehow contradicts the conventional lubrication theory, where the theory will predict an opposite result. An explanation of this contradiction will be given in section 5.5.
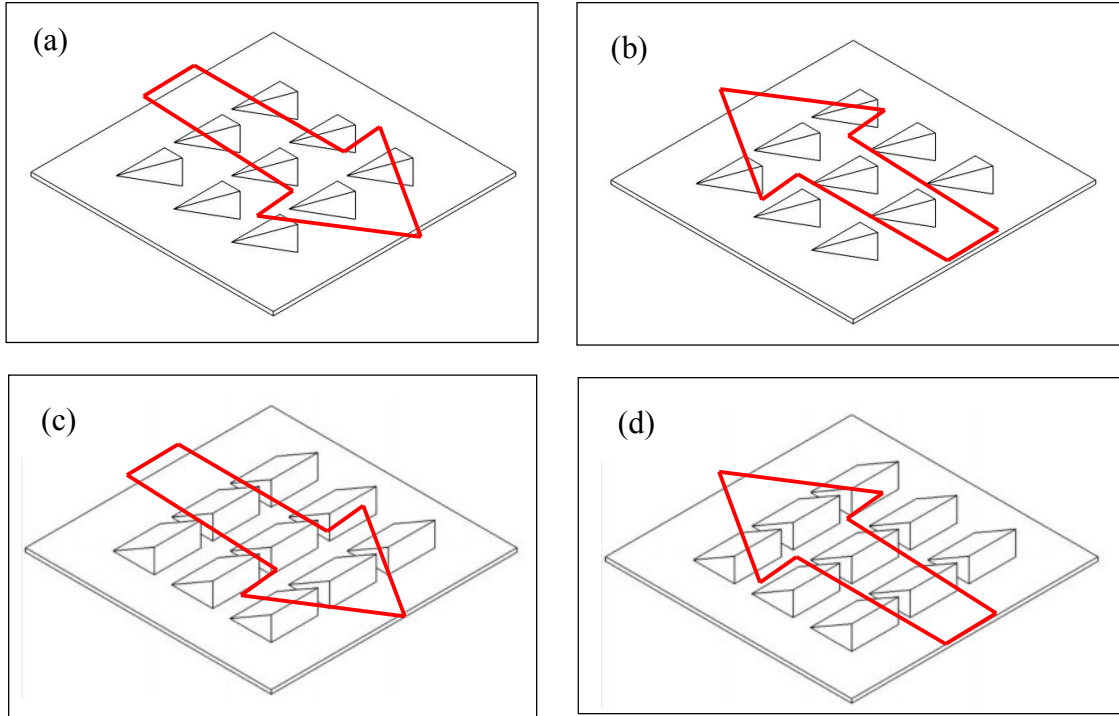
Fig. 5.4 Indication of the flow direction
(a, b on the triangular asperity surface; c, d on the square asperity surface)
a, c. the upper surface travels to the +x direction, the fluid is pushed into the convergent gap;
b, d. the upper surface travels to the–x direction, the fluid is dragged out of the convergent gap.

Phenomenon 3: The square asperity has a larger friction force than the triangular asperity when the upper surface travels along the +x direction, while this becomes opposite when the upper surface travels along the -x direction. The frictional difference (43.3%) between the +x and the −x directions with the regular square asperity is larger than that (14.2%) with the regular triangular aspertiy.

The reason behind these phenomena will be explained in the next section.

5.5 Mechanisms for Directional Friction

In this section, the underlying reason behind the three phenomena 1-3 as observed based on the simulation and described in section 5.4 will be discussed. The discussion is based on the following two proposed theories or mechanisms:

Theory 1: when the upper surface starts to move rightward (Fig. 5.5), a layer of liquid molecules which are closest to the upper surface will move with it, and these molecules will pass the momentum they have acquired from the upper surface to layers of molecules, which are not close to the upper surface by diffusion. In this way, if the upper surface keeps moving, all fluid molecules in the fluid (except those closest to the fixed lower surface) will move rightward at a certain speed. The molecules respond to dragging on the upper surface in this process. The friction force is the accumulation of these dragging forces.
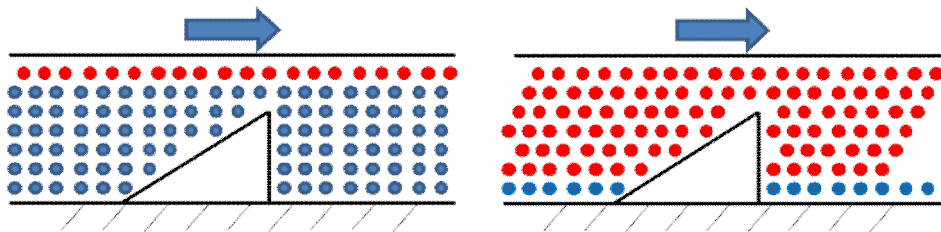
Fig. 5.5 Movement of the upper surface and the molecules
(Red dots represent moving molecules; blue dots represent static molecules)

The movement of the upper surface will keep dragging the fluid away from the fluid domain. In this situation, within some areas of the domain where there is a sufficient supply of fluid, the amount of fluid molecules will not reduce. However, within some other areas of the domain where there is not a sufficient supply of fluid due to the blockage of the asperities, the amount of

fluid molecules will reduce. The reduction of the fluid molecules will then lead to two possible situations. In the first situation, the fluid cannot fill all the space it has originally taken. The gas dissolved in the fluid will then expand to take over a certain portion of that space, which leads to the cavitation or film rupture situation. In the second situation, reduction of the fluid molecules causes some portions of the fluid to vaporize and the vaporized gas will then fill the space, which leads to the cavitation. In the both situations, with reduction of the fluid molecules and formation of the cavitation, the pressure, which is the accumulation of thermal dynamic effect of millions of fluid molecules, will reduce. The friction force, which is the accumulation of the drag from millions of fluid molecules, will reduce accordingly. Along with the discussion above, a guideline for understanding is established, as presented in Fig. 5.6:

More blockages from the asperity

Less fluid supply

More film ruptured areas

Less friction on the upper surface

Fig. 5.6 General guideline with theory 1

Theory 2: the smaller the gap between two surfaces, the lager the friction force will be on the upper surface. This is because friction force on the upper surface is proportional to shear strain, which is further proportional to velocity gradient along the gap direction. The smaller the gap, the larger the velocity gradient will be.

The phenomena are now ready to be explained by the theories. For Phenomenon 2, it can be explained by theory 1. As shown in Fig. 5.4, along the direction indicated by the arrow shown in Fig. 5.4a (i.e., the +x direction), the asperity forms a shape that has less blockage than that along the direction indic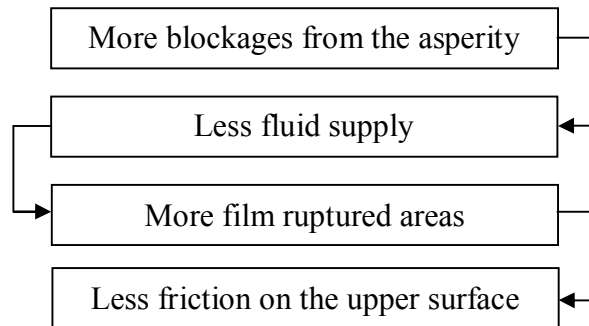ated by the arrow in Fig. 5.4b (i.e., the -x direction). So it is more difficult for the fluid to flow in Fig. 5.4b than to flow in Fig. 5.4a. Thus, there will be less fluid supply and more film ruptured areas in Fig. 5.4b than that in Fig. 5.4a. According to the guideline of Fig. 5.6; more film ruptured areas will lead to less friction force on the upper surface. Therefore, there will be less friction force on the upper surface when the upper surface travels along the −x direction (Fig. 5.4b) than that along the +x direction (Fig. 5.4a). This discussion also explains why directional friction is feasible on the surface with triangular RAAs, and the same is true for the surface with square asperities, shown in Fig. 5.4c, d.

The above logic is further supported by the simulation of the pressure distribution on the upper surface. Fig. 5.7 shows the pressure distribution on the upper surface when the lower surface has triangular RAAs (Fig. 5.7a and b) and square RAAs (Fig. 5.7c and d). In Fig. 5.7, the blue area is the area where the pressure is below the ambient level (i.e., film ruptured area). Fig. 5.7a shows the pressure distribution on the upper surface when the flow travels along the +x direction, and the blue area counts about 31.2% of the total area, while in Fig. 5.7b, it shows the pressure distribution when the fluid travels along the −x direction, where the blue area counts about 40.7% of the total area. Therefore, the friction force for Fig. 5.4a will be larger than that for Fig. 5.4b. Likewise, for the square RAA surface, the blue area in Fig. 5.7c (the +x direction) counts about 27.3%, and the blue area in Fig. 5.7d (the -x direction) counts about 60.1%. In short, the

simulation shows that the fluid traveling along the –x direction contains more cavitation area than that the fluid traveling along the +x direction.
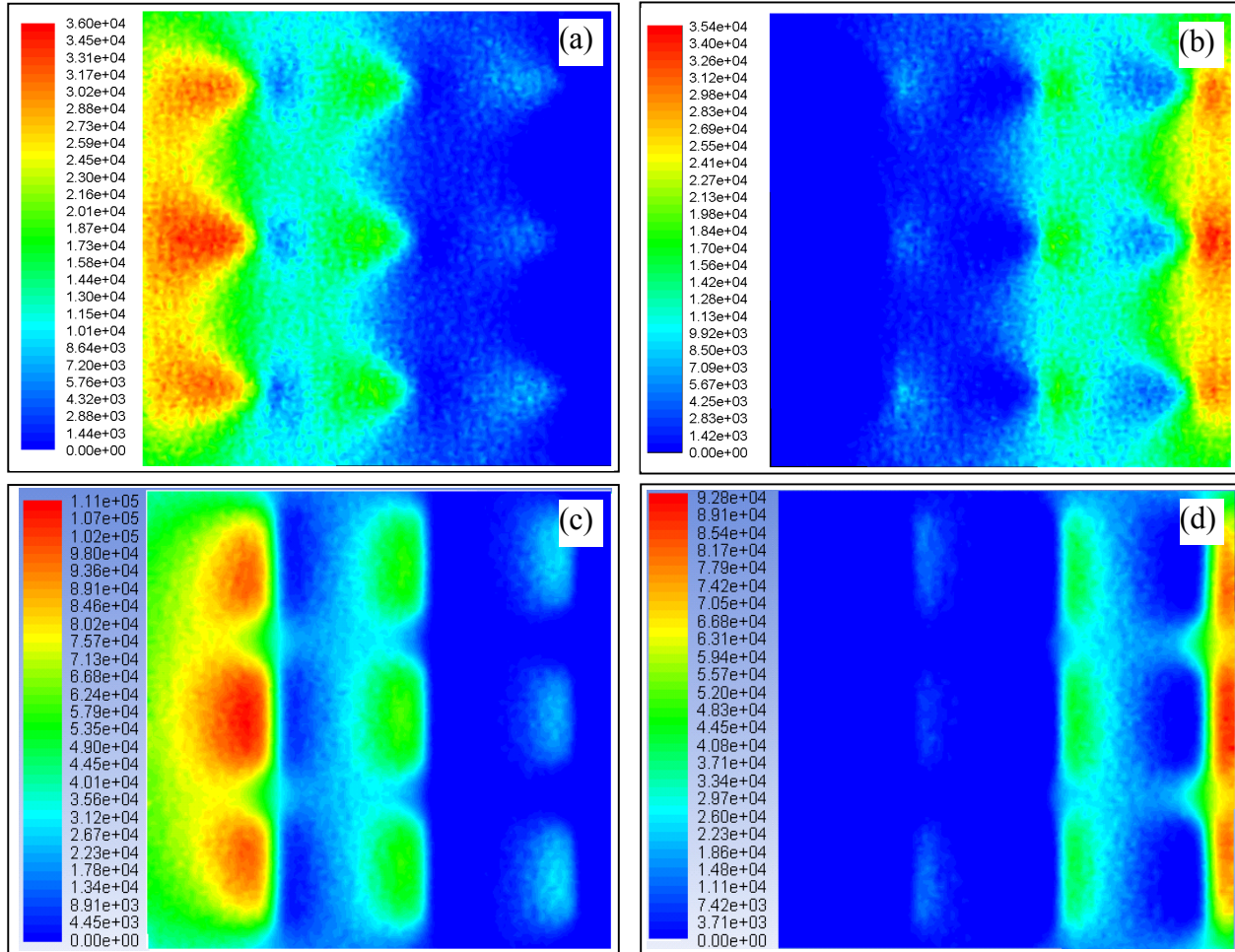

Fig. 5.7 Pressure distribution on the upper surface
(a, c): when the upper surface travels towards +x direction; (b, d): towards –x direction
(a, b): on the surface with triangular asperities; (c, d): on the surface with square asperities

The approach to explaining the underlying mechanism for Phenomenon 2 can be applied to that for Phenomenon 1.

As mentioned above in section 5.4, Phenomenon 2 contradicts the conventional lubrication theory. This is because in the situation studied in this thesis, distance D between two surfaces is fixed. In the conventional lubrication theory, if the movement of the surface(s) pushes the lubricant into the convergent gap, the friction force reduces due to the hydrodynamic pressure which will lift the upper surface and then increase the gap between the surfaces. The friction between the two surfaces will change from a boundary friction state to mixed friction state, and to fully lubricant friction state. Usually, the friction force is larger when two surfaces are in the boundary or mixed friction state, so the friction force will reduce if two surfaces are separated into a fully lubricated state by the hydrodynamic pressure. However, if the movement of the surface(s) changes to the opposite direction, no hydrodynamic lubrication is established; instead, "negative" pressure (due to cavitation) may break the lubricant film, and consequently friction force increases. In this thesis, the distance between two surfaces is fixed and they are always in a fully lubricated state, so the situation here is different from that concerned in the conventional lubricant theory.

For Phenomenon 3, the square asperity surface has a larger friction force than the triangular one does when the upper surface travels along the +x direction, and this could be explained by theory 2. As for the square asperity, there are more surface areas that have a small gap than those for the triangular one. So there will be more friction force on the upper surface with the square asperity when the upper surface travels along the +x direction (Fig. 5.4c). The fact that the square asperity surface has a smaller friction force than the triangular one when the upper surface travels along the –x direction could be explained by theory 1. Comparing Fig. 5.4b and d, it can be seen that the triangular asperity forms a shape that has less blockage of the fluid than the

square one does. Following the guidelines of theory 1, the square asperity will have a smaller friction force than the triangular asperity.

Furthermore, when it comes to the situation where there are RAAs on both surfaces (upper and lower), theory 1 will be able to give clues to answer the question "if the directional friction is realizable or not" and "what direction will have a larger friction force". These clues can be generated by analyzing the structure of the fluid domain and find out if the blockage of the asperities will cause different blockages on the fluid flow and what direction will block more.

5.6 Conclusions

In this chapter, the NS-HSC model was applied to the surface with triangular RAAs and the surface with square RAAs. Friction forces on these surfaces were obtained through simulation when the upper surface travels along the two opposite directions (i.e., +x and -x). The study proposed two theories with which to explain the flow behavior in relation to friction. The simulation concludes:

(a) Friction force is different when the upper surface travels toward two opposite directions on a fully lubricated surface with RAAs. Directional friction is presented on the fully lubricated surface with RAAs.

(b) Friction force will be smaller when the movement of the upper surface drags the lubricant film out of the convergent gap than when it pushes the lubricant into the convergent gap.

(c) The degree of directionality of friction force (i.e., the difference between friction forces induced associated with two opposite directions) is larger on the square RAA surface than that on the triangular RAA surface.

.

CHAPTER 6 CONCLUSION AND FUTURE WORK

6.1 Overview of the Thesis

In the first chapter of this thesis, a general background necessary to describe the motivation of the study was presented, which includes the concepts such as friction uniformity, directional friction and regular isotropic/anisotropic asperity. These concepts are perhaps new to the current literature. The understanding of these concepts allows the motivation of the study to be introduced, i.e., a need to understand the structure-function relationship for directional friction for regular anisotropic asperity (RAA) surfaces. The overall objectives of the study followed, namely: (1) to develop a CFD model for computing lifting force and friction force of a flat surface moving on the top of a RAA surface; and (2) to study the structure-function relationship of directional friction for fully lubricated RAA surfaces.

In the second chapter of this thesis, related work was discussed, which includes: a) the work related to the surface with RAAs, b) the work related to the friction uniformity, and c) the work related to the modeling of inter-asperity flow. The analysis of these works has further justified the research questions and objectives of this thesis, presented in the first chapter.

In the third chapter of this thesis, the NS-HSC model was established, which allows for the computation of both lifting force and the friction force on a fully lubricated surface with RAAs.

The discussion there followed: set-up of a scheme upon which to generate a mesh, choice of the governing equation (i.e., Navier-Stokes equation), determination of the boundary condition, and description of cavitation (i.e., Half-Sommerfeld Condition).

In the fourth chapter of this thesis, the NS-HSC model was verified with the data from the literature, and specifically, the verification was conducted by comparing the friction force result predicted by the NS-HSC model with the experimental result from the literature and the result predicted by the RE (Reynolds Equation)-HSC model reported in the same literature. The comparison demonstrated that the NS-HSC model is better than the RE-HSC model. A discussion on the comparison result followed to explain the underlying reason.

In the fifth chapter of this thesis, the effect of the RAAs on the directional friction force was studied with the NS-HSC model. In particular, the model was applied to two shapes of the RAA with one being a triangular shape and the other being a square shape. The study has provided strong evidence on the presence of directional friction on fully lubricated RAA surfaces. As well, a theory which can provide a qualitative prediction of directional friction force for a fully lubricated RAA surface was proposed and described in this chapter.

6.2 Conclusion and Contribution

This thesis study concludes:

(1) The Navier-Stokes equation should be applied to the problem of modeling flow behavior of the fluid on a fully lubricated RAA surface, whereas the Reynolds equation is not applicable to this problem.

(2) The Half-Sommerfeld condition can provide a reasonable approximate description of fluid cavitations that can happen to a fully lubricated RAA surface.

(3) There is the directional friction behavior exhibited on a fully lubricated RAA surface, and this behavior is sensitive to the structure of the RAA surface.

(4) There is a sound computational support to a theory proposed in this thesis, which is based on the very intuitive flow behavior when the fluid is pushed to a smaller space and dragged to a larger space.

The major contributions of this thesis are:

(1) The first work to model directional friction for a fully lubricated RAA surface, which provides theoretical evidence on the presence of directional friction on such surfaces.

(2) The first work to combine the NS equation and HSC to model the flow behavior of the fluid within a gap that is fully lubricated and "uneven" where the fluid density may change due to cavitations.

(3) A preliminary theory that gives qualitative knowledge about the structure-function relationship for directional friction on a fully lubricated RAA surface. The theory can provide a guideline to design RAA surfaces for a required behavior of directional friction on a fully lubricated RAA surface.

6.3 Future Work

This thesis presents a primary research on the effect of regular asperities on the frictional behavior and theoretically demonstrates that directional friction is feasible on a fully lubricated surface with RAAs. However, there are still some issues which need to be addressed in the future research and they are discussed in the following:

(1) Experimental verification of directional friction on a fully lubricated surface with RAAs. This will also be useful to further validate the NS-HSC model. It is noted that the current validation of the NS-HSC model is based on a relatively "coarse" test bed which is not much in control.

(2) Improvement of modeling cavitation. The model developed in this thesis takes the Half-Sommerfeld condition to describe the cavitation region. However, the way to combine the NS and HSC is somewhat "sequential": first apply the NS and then apply HSC to modify the NS's result. A "concurrent" use of the NS and HSC would be in favor, as the fluid behaves in the real-world system concurrently. One of the possible solutions is to employ the density function in the NS and HSC equations.

(3) Understanding the size effect on the degree of friction directionality. In this thesis, two surfaces with different RAAs were studied, and the result of the study reveals that the degree of friction directionality is higher for the square RAA surface than that for the triangular RAA surface. However, there is no study on the size effect which may also play a role in

contributing to the degree of friction directionality, which is worth study in the future.

(4) Development of models for directional friction on non-lubricated surfaces with RAAs and on mixed-lubricated surfaces with RAAs. The current friction model in the literature is based on a surface with irregular asperities, and modeling of friction on the regular surface is a promising future work.

(5) Development of more efficient fabrication techniques for surfaces with regular asperities (isotropic or anisotropic). The current methods (e.g., use of the LIGA process) of fabricating regular asperities on the surface is time consuming and economically unviable.

(6) Investigation of the tribological properties such as wear and adhesion for regular asperity surfaces. This thesis only considers friction behavior of a surface. It is known that the surface of a material has many other uses, such as adhesion and adsorption. It is expected that these properties have some profound change for regular asperity surfaces compared with irregular asperity surfaces.

LIST OF REFERENCES

[1]   Aksak, B., Murphy, M.P., Sitti, M., (2007). Adhesion of Biologically Inspired Vertical and Angled Polymer Microfiber Arrays. Langmuir. 23: 3322-3332.

[2]   Ando, Y., Ino, J., (1998). Friction and pull-off forces on submicron-size asperities. Wear. 216: 115-122.

[3]   Ando, Y., (2000). Wear tests and pull-off force measurements of single asperities by using parallel leaf springs installed on an atomic force microscope. ASME transactions, Journal of tribology, 122: 639-645.

[4]   Brajdic-Mitidieri, P., Gosman, A.D., Ioannides, E., Spikes, H.A., (2005). CFD Analysis of a low friction pocketed pad bearing. Transaction of ASME, Journal of Tribology. 127: 803-812.

[5]   Bhushan, B., (2002). Introduction to Tribology. John Wiley & Sons, New York. USA.

[6]   Chvedov, D., Jones, R., Rosenfeld, A., (2003). Effect of lubricant quantity and surface topography on the frictional behaviour of can body stock. Tribology Transactions 46 (3), 339–347.

[7]   Dickrell, P.L., Sinnott, S.B., Hahn, D.W., Raravikar, N.R., Schadler, L.S., Ajayan, P.M., Sawyer, W.G., (2005). Frictional anisotropy of oriented carbon nanotube surfaces. Tribology Letters 18 (1), 59–62.

[8]   Etsion, I., Halperin, G., (2002). A laser surface textured hydrostatic mechanical seal. Tribology Transactions 45(3): 430-434.

[9]   Feldman, Y., Kligerman, Y., Etsion, I., (2006). A hydrostatic laser surface textured gas seal.

Tribology letters. 22(1): 21-28.

[10] Gatzen, H.H., Beck, M., (2003). Investigations on the friction force anisotropy of the silicon lattice. Wear 254 (11):1122–1126.

[11] Gellman, A.J., Ko, J.S., (2001). The current status of tribological surface science. Tribology Letters. 10 (1-2): 39-44.

[12] Greenwood, J.A., Williamson, J.B.P., (1966). Contact of nominally flat Surface. Proceedings of the royal society of London. Series A, Mathematical and Physical Sciences. 295(1442): 300-319.

[13] Greenwood, J.A., (1984). A unified theory of surface roughness. Proceedings of the royal society of London. Series A, Mathematical and Physical Sciences. 393: 133-157.

[14] Hamrock, B.J., Schmid, S.R. et al., (2004). Fundamentals of Fluid Film Lubrication. Marcel Dekker Inc. New York.

[15] Harp, S.R., Salant, R.F., (2001). An averaged flow model of rough surface lubrication with inter-asperity cavitation. Journal of Tribology. 123(1): 134-143.

[16] Hazel, J., Stone, M., Grace, M.S., Tsukruk, V.V., (1999). Nanoscale design of snake skin for reputation locomotions via friction anisotropy. Jounral of Biomechanics. 32: 477-484.

[17] He, Q.C., Curnier, A., (1993). Anisotropic dry friction between two orthotropic surfaces undergoing large displacements. European Journal of Mechanics A/Solids. 12: 631-666.

[18] Hisada, K., Knobler, C.M., (2002). Microscopic friction anisotropy and asymmetry related to the molecular tilt azimuth in a monolayer of glycerol ester. Colloids and Surfaces A: Physicochemical and Engineering Aspects. 198-200: 21–30.

[19] Hori, Y., (2006). Hydrodynamic Lubrication. Springer-Verlag, Tokyo, Japan.

[20] Hutton, T.J., Johnson, D., McEvaney, B., (2001). Effects of fiber orientation on the

tribology of a model carbon–carbon composite. Wear. 249 (8): 647–655.

[21] Ike, H., (1996). Properties of metal sheets with 3-D designed surface micro-geometry prepared by special rolls. Journal of material processing technology. 60: 363-368.

[22] Jakobsson, B., Floberg, L., (1957). The finite journal bearing considering vaporization. Transactions of Chalmers University of Technology. Gothenburg, Sweden. P.190.

[23] Kovalchenko, A., Ajayi, O., Erdemir, A., Fenske, G., Etsion, I., (2005). The effect of laser surface texturing on transitions in lubrication regimes during unidirectional sliding contact. Tribology International. 38: 219-225.

[24] Longuet-Higgins, M.S., (1957). The statistical analysis of a random, moving surface. Philosophical Transactions of the Royal Society of London. Series A, Mathematical and Physical Science. 249(966): 321-387.

[25] Lucas, M., Zhang, X.H., Palaci, I., Klinke, C., Tosatti, E., Riedo, E., (2009). Hindered rolling and friction anisotropy in supported carbon nanotubes. Nature Materials. 8: 876 – 881.

[26] Mancinelli, C.M., Gellman, A.J., 2004. Friction anisotropy at Pd(100)/Pd(100) interfaces. Langmuir. 20(5): 1680–1687.

[27] Mateescu, G., Ribbens, C.J., Watson, T.L., Wang, C.Y., (1999). Effect of a saw tooth boundary on Couette flow. Computers and Fluids. 28: 801-813.

[28] Mishra, C., Peles, Y., (2005). Cavitation in flow through a micro-orifice inside a silicon microchannel. Physics of Fluids. 17:013601.

[29] Mishra, C., Peles, Y., (2006). An experimental investigation of hydrodynamic cavitation in micro-Venturis. Physics of Fluids. 18:103603.

[30] Moromuki, N., Nishi, D., Uchiyama, K., (2001). Textured surface produced by anisotropic

etching of silicon and its frictional properties. Initiatives of Precision Engineering at the Beginning of a Millennium, 10th International Conference on Precision Engineering (ICPE) July 18–20, 2001, Yokohama, Japan.

[31] Morz, Z., Stupkiewicz, S., (1994). An anisotropic friction and wear model. International Journal of Solids and Structures. 31(8): 1113-1131.

[32] Murphy, M.P., Aksak, B., Sitti, M., (2007). Adhesion and anisotropic friction enhancements of angled heterogeneous micro-fiber arrays with spherical and spatula tips. Journal of Adhesion technology. 21(12-13): 1281-1296.

[33] Ohtani, T., Kamasaki, K., Tanaka, C., (2003). On abrasive wear property during three-body abrasion of wood. Wear. 255 (Part I): 60–66.

[34] Ohzono, T., Fujihira, M., (2000). Simulations of friction anisotropy on ordered organic monolayer. Tribology Letters. 9: 63–67.

[35] Okabe, S., Yokoyama, Y., and Boothroyd, G., (1988). Analysis of Vibratory Feeding Where the Track has Directional Friction Characteristics. The International Journal of Advanced Manufacturing Technology, 3 (4): 73-85.

[36] Olsson, K.O., (1965). Cavitation in dynamically loaded bearing. Transaction of Chalmers University of Technology. Guthenburg, Sweden. P. 308.

[37] Petterson, U., Jacobson, S., (2006). Tribological texturing of steel surfaces with a novel diamond embossing tool technique. Tribology international. 39: 695-700.

[38] Qi, Y., Cheng, Y.T., Cagin, T., Goddard, W.A., (2002). Friction anisotropy at Ni(100)/(100) interfaces: Molecular dynamics studies. Physical Review B. 66: 085420.

[39] Qiu, Y., Khonsari, M.M., 2009. On the prediction of cavitation in dimples using a mass-conservative algorithm. Transaction of ASME, Journal of Tribology. 131: 041702-1.

[40] Rhaiem, S., Dammak, M., Shirazi-Adl, A., Mesfar, W., Maalej, A., (2004). Combined Experimental and Finite Element Studies of Anisotropic Friction. Journal of Material Science and Technology. 20(Suppl. 1): 11-14.

[41] Ryk, G., Kilgerman, Y., Etsion, I., (2002). Experimental Investigation of Laser Surface Texturing for Reciprocating Automotive Components. Tribology Transactions. 45: 444-449.

[42] Sahlin, F., (2005). Hydrodynamic Lubrication of Rough surfaces. Licentiate Thesis. Lulea University of Technology, Sweden.

[43] Sahlin, F., Glavatskih, S.B., Almqvist, T., Larsson, R., (2005). Two-Dimensional CFD-Analysis of Micro-Patterned Surfaces in Hydrodynamic Lubrication. Transactions of the ASME, Journal of Tribology. 127: 96-102.

[44] Sakata, F.Y., Santo, A.M.E., Miyakawa, W., Riva, R., Lima, M.S.F., (2009). Influence of laser surface texturing on surface micro-structure and mechanical properties of adhesive joined steel sheets. Surface Engineering. 25(3): 180-186.

[45] Schweizer, B., (2009). Numerical Approach for solving Reynolds Equation with JFO boundary conditions incorporating ALE techniques. Journal of Tribology 131(1): 011702-1-14.

[46] Shastry, A., Case, M.J., Bohringer, K.F., (2006). Directing droplets using micro-structured surfaces. Langmuir. 22: 6161-6167.

[47] Shi, Y.J., Yao, Z.Q., Liu, F., Qi, Y.G., (2008). Numerical investigation on laser-produced microstructure of metal under non-melting condition. Applied Surface Science. 254: 7421-7426.

[48] Siripuram, R.B., Stephens, L.S., (2004). Effect of Deterministic Asperity Geometry on

Hydrodynamic Lubrication. Transaction of ASME: Journal of Tribology. 126: 527-534.

[49] Stephens, L.S., Siripuram, R., Hayden, M., McCartt, B., (2004). Deterministic Micro Asperities on Bearings and Seals Using a Modified LIGA process. Transaction of ASME, Journal of Engineering for Gas Turbines and Power. 126: 147-154

[50] Tang, Y.J., Li, Y.S., Yang, Q., Hirose, A., (2010). Fabrication and orientation control of diamond nano tips by broad ion beam etching. Journal of Physics D: Applied Physics. 43.

[51] Wang, X.L., Kato, K., Adachi, K., Aizawa, K., (2001). The effect of laser texturing of SiC surface on the critical load for the transition of water lubrication mode from hydrodynamic to mixed. Tribology International. 34: 703-711.

[52] Wang, X.L., Kato, K., (2003). Improving the anti-seizure ability of SiC seal in water with RIE texturing. Tribology Letters. 14(4): 275-280.

[53] Yamamoto, Y., Hashimoto, M., (2004). Friction and wear of water lubricated PEEK and PPS sliding contacts, Part 2. Composites with carbon or glass fibre. Wear. 257 (1–2): 181–189.

[54] Yim, S., Jeona, D.Y., (2009). Capsular Microrobot using Directional Friction Spiral. 2009 IEEE International Conference on Robotics and Automation Kobe International Conference Center Kobe, Japan, May 12-17.

[55] Zhang, H.S., Kyriakos, K., (2009). Scale-dependent nanomechanical behaviour and anisotropic friction of nanotextured silicon surfaces. Journal of Material Research. 24(10): 3038-3043.

[56] Zhang, Q.S., (2008). Development and Characterization of a Novel Piezoelectric-Driven Stick-Slip Actuator with Anisotropic-Friction Surfaces. M.Sc. thesis, University of Saskatchewan.

[57] Zhang, W.J., Chen, X.B., Yang, Q., (2004). On the study of Slip-Stick actuator. A Proposal to NSERC Strategic Project Grant Program.

[58] Zmitrowicz, A., (1981). A theoretical model of anisotropic dry friction. Wear. 73: 9-39.

[59] Zmitrowicz, A., (1992). Constitutive modeling of centrosymmetric and non-centrosymmetric anisotropic friction. International Journal of Solids and Structures. 29(23): 3025-3043.

[60] Zmitrowicz, A., (1999). An equation of anisotropic friction with sliding path curvature effects. International Journal of Solids and Structures. 36(19): 2835-2848.

[61] Zmitrowicz, A., (2006). Models of kinematics dependent anisotropic and heterogeneous friction. International Journal of Solids and Structures. 43: 4407–4451.

APPENDIX A: UDF FOR HSC APPLICATION

```
/********************************************************************
UDF for modify the pressure when the pressure is less than zero (i.e., the application of HSC),
    and calculate the surface area where pressure >0Pa
********************************************************************/



#include "udf.h"
#include "mem.h"
#include "metric.h"

/* ******************************************************************
System defined macron which can be execute upon the demand of the user. "Pressure_adjust is
    the name of the function defined
********************************************************************/


DEFINE_ON_DEMAND (pressure_adjust)

{

/********************************************************************
Claim the variables involved in the function
********************************************************************/


   Domain *d;          /* Pointer to the fluid domain*/
   Thread *t;
   Thread *tt;
   cell_t c;           /* Define a cell variable */
   face_t f;           /* Define a cell face variable */
   int ID=52;          /* Integer "52" is the fluid domain number, this value varies with the
                          different simulations */
```

```
real x[ND_ND]={1,1,1};
real asum=0;
real NV_VEC(A);
d=Get_Domain(1);
tt=Lookup_Thread(d,ID);
```

```
/************************************************************************
Search the pressure values of the cells, if the pressure is smaller than 0 Pa, switch it back to 0 Pa.
*************************************************************************/
```

```
thread_loop_c(t,d)
{
begin_c_loop(c,t)
   if (C_P(c,t)<0)        /* If the pressure within the fluid domain is smaller than 0 Pa, switch it
                              back to 0 Pa */

      {C_P(c,t)=0;}
end_c_loop(c,t)
}
thread_loop_f(t,d)
{
begin_f_loop(f,t)      /* If the pressure on the out surface of the fluid domain is smaller than 0
                           Pa, switch it back to 0 Pa */

      if (F_P(f,t)<0)
      {F_P(f,t)=0;}
   end_f_loop(c,t)
}
```

```
/************************************************************************
Calculate the area where pressure is larger than 0 Pa on the upper surface
*************************************************************************/
```

```
begin_f_loop(f,tt)               /* Search over the cell faces that are on the upper surface */
   if (F_P(f,tt)>0)              /* See if the pressure is larger than 0 Pa */
   {
        F_AREA(A,f,tt);     /* Get the amount of the area of the cell faces  */
        asum+=NV_MAG(A); /* Accumulate the amount of these area */
```

```
    }
  end_f_loop(f,t)
  printf("%f",asum);    /* Report the total amount of the area where pressure is larger than 0 */
}
```